International Journal of Biological Macromolecules 214 (2022) 554–567

Contents lists available at ScienceDirect

International Journal of Biological Macromolecules

journal homepage: www.elsevier.com/locate/ijbiomac

Different Kraft lignin sources for electrospun nanostructures production: Influence of chemical structure and composition

Luisa García-Fuentevilla [a], José F. Rubio-Valle [b], Raquel Martín-Sampedro [a], Concepción Valencia [b], María E. Eugenio [a,*], David Ibarra [a]

[a] Forest Research Center, INIA-CSIC, Ctra. de la Coruña, km 7.5., 28040 Madrid, Spain
[b] Pro2TecS—Chemical Process and Product Technology Research Centre, Departamento de Ingeniería Química, ETSI, Campus de "El Carmen", Universidad de Huelva, 21071 Huelva, Spain

ARTICLE INFO

Keywords:
Kraft lignin
Chemical characterization
Electrospinning

ABSTRACT

This work focuses on the structural features and physicochemical properties of different Kraft lignins and how they can influence the electrospinning process to obtain nanostructures. Structural features of Kraft lignins were characterized by nuclear magnetic resonance, size exclusion chromatography, fourier-transform infrared spectroscopy, and thermal analysis, whereas chemical composition was analyzed by standard method. The addition of cellulose acetate (CA) improves the electrospinning process of Kraft lignins (KL). Thus, solutions of KL/CA at 30 wt% with a KL:CA weight ratio of 70:30 were prepared and then physicochemical and rheologically characterized. The morphology of electrospun nanostructures depends on the intrinsic properties of the solutions and the chemical structure and composition of Kraft lignins. Then, surface tension, electrical conductivity and viscosity of eucalypt/CA and poplar/CA solutions were suitable to obtain electrospun nanostructures based on uniform cross-linked nanofibers with a few beaded fibers. It could be related with the higher purity and higher linear structure, phenolic content and S/G ratios of lignin samples. However, the higher values of electrical conductivity and viscosity of OTP/CA solutions resulted in electrospun nanostructure with micro-sized particles connected by thin fibers, due to a lower purity, S/G ratio and phenolic content and higher branched structure in OTP lignin.

1. Introduction

One of the most important challenges in today's society is the implementation of a sustainable bioeconomy aiming at mitigating both greenhouse gas (GHG) emissions and fossil fuels consumption. In this scenario, lignocellulosic biomass is an abundant and widely distributed resource considered as an important renewable alternative to fossil fuels for the production of materials, chemicals and energy [1]. Many different lignocellulosic materials, including dedicated crops and agriculture residues, are potentially suitable for lignocellulosic biomass supply. Among crops, poplar is a species naturally distributed throughout the northern hemisphere, with an exceptional significance due to high biomass quality, high resistance to diseases and pests, high tolerance to salinity and adaptation to fertilizer and water limitations. The suitability of this species for biomass production is widely supported in different cultivation areas [2] and especially in the Mediterranean area [3]. Similarly, one of the most abundant and cheapest lignocellulosic residues also generated in Mediterranean countries is olive tree pruning, with an estimated average production of 3000 kg/ha per year worldwide [4]. This material is frequently disposed to maintain fields clean and to avoid the spread of plant diseases by grinding, spreading on fields or burning, resulting in environmental impact and economic costs.

Cellulose is the most appreciated component of both lignocellulosic materials. It has been widely evaluated for its transformation to bioethanol [5,6], cellulosic pulp and advanced materials such as nanofibrillated cellulose among others [7,8]. However, for other lignocellulosic components, such as lignin, not as many ways of valorization have been found.

Lignin is considered a renewable resource with the potential to produce extensive chemicals and materials [9,10]. It mainly occurs in natural plants in the form of aromatic polymer with the main building blocks of *p*-hydroxyphenyl (H), guaiacyl (G), and syringyl (S) phenylpropane units and the chemical linkages of aryl-ether and

* Corresponding author.
E-mail address: mariaeugenia@inia.csic.es (M.E. Eugenio).

https://doi.org/10.1016/j.ijbiomac.2022.06.121
Received 21 March 2022; Received in revised form 13 June 2022; Accepted 17 June 2022
Available online 22 June 2022

carbon-carbon bonds [11]. Currently, pulp and paper industry is the main supplier of lignin, being Kraft pulping the most extended technology with an estimated average production of around 55–90 million tons per year worldwide [12,13]. This lignin is currently underexploited, being usually burned to produce energy to cover part of the needs of the pulping industry. However, about 60 % more residual lignin is generated than what is required to meet pulping mill energy necessities [14]. Therefore, different research projects are accelerating to find feasible opportunities for valorising this residual lignin into high value-added products [15–17].

Among the different lignin valorization ways, micro and nanosize lignin has recently gained interest due to its improved properties compared to currently available standard lignin. A wide range of applications is reported in the literature such as batteries, supercapacitors, fuel cells, structural composites, and filtration devices [18,19]. In this sense, electrospinning is a well-established technique for the fabrication of lignin nanofibers [20,21]. Although this process was patented more than eighty years ago [22] until relatively recently, no particular attention had been paid to this technology. Its great interest comes from the extraordinary possibilities offered by engineered nanostructures due to their combination of high porosity, small size and high surface-to-volume ratio [23,24].

The production of lignin nanofibers by electrospinning is still underdeveloped for several reasons due to lignin properties. Among them, they may include the heterogeneity of its chemical composition, its branched structure, or the presence of low-molecular-weight compounds resulting from the lignin degradation process. All these features, very common in Kraft lignins, result in non-uniform nanostructures formed by particles or globules distributed along the filament, known as BOAS (beads on-a-string) when lignin is electrospun [25], because the lignin cannot create sufficient chain entanglements within the solution [26]. Nevertheless, given the industrial and scientific relevance of Kraft lignins to fabricate high-value added products, it is of great significance to enable Kraft lignins for lignin nanofibers production. Thus, in order to address this challenge a deeper knowledge of the structure and properties of different available Kraft lignins is necessary [27,28]. Moreover, several strategies have been developed to improve the lignin electrospinnability, including the use of different polymers as doping agents, such as polyethylene oxide (PEO) [25,29,30], polyvinyl alcohol (PVA) [31,32], polyvinylpyrrolidone (PVP) [33,34], and cellulose acetate (CA) [35]. It is worth highlighting the latter dopant because it generates fibers with relative ease, and for its properties such as biodegradability, biocompatibility and renewable resource [35–37].

Taking into account the above, the present work aimed to study the structural features and physicochemical properties of different Kraft lignins sources, i.e., from poplar, olive tree pruning and eucalypt (as reference), and how they can influence the electrospinning process, together with cellulose acetate as doping, to obtain high-quality lignin nanostructures. Understanding the structural features and physicochemical properties of these Kraft lignins would help to address the production of high-quality nanofibers from them. Furthermore, it would optimize the application of these nanostructures in a forthcoming work as vegetable oil thickening agents for lubricant industry. Thus, the high porosity, small size and high surface/volume ratio of lignin nanofibers may lead to the formation of three-dimensional networks with a great ability to promote physical interactions between the oil and the nanofibers [33]. Then, the development of these oil thickeners based on lignin nanofibers represents a key challenge in terms of environmentally friendly substitutes to synthetic compounds derived from fossil fuels or metal soap-based thickeners, which are either not biodegradable or require highly toxic production processes.

2. Materials and methods

2.1. Raw materials and chemicals

Olive tree (*Olea europaea*) pruning (OTP) residue was kindly supplied by the University of Jaén (Spain). An autochthonous clone of poplar (*Populus alba* L.) from the Guadalquivir valley, PO-10-10-20, was kindly provided by Silviculture and Forest Management Department of INIA, CSIC (Madrid, Spain). Poplar samples (3 years old) were collected from plantations in the central area of Spain, chipped, homogenized, and stored until used. Eucalypt (*Eucalyptus globulus*) lignin was provided by ENCE pulp mill (Pontevedra, Spain). This lignin was used as a reference and it was obtained by acid precipitation (pH lowered to 2.5 with concentrated sulphuric acid) from the Kraft black liquor.

Cellulose acetate (CA) (M_n = 30,000 g/mol by gel permeation chromatography, 39.8 wt% acetyl) was provided by Sigma-Aldrich S.A. (Germany) and used as a dopant in the polymeric solution for the electrospinning process. In addition, *N*, *N*-dimethylformamide (DMF) and acetone (Ac), supplied by Sigma Aldrich S.A. (Germany), were used as solvents to prepare lignin/CA solutions.

Finally, all other chemicals were reagent-grade and purchased from Panreac (Barcelona, Spain), Fisher Scientific (Madrid, Spain) or Sigma-Aldrich (Madrid, Spain).

2.2. Kraft pulping and lignin recovery

Kraft pulping of olive tree pruning and poplar materials was carried out in a cylindrical 15 L batch reactor with a jacket-type electrical heater controlled by a computer. The reactor was fitted with a rotating axle to ensure proper agitation. OTP was cooked under the following conditions: 175 °C, 90 min, 20 % active alkali, 25 % sulfidity and 5:1 liquid/solid ratio, according to Fillat et al. [7]; whereas for poplar the conditions were: 170 °C, 120 min, 17 % active alkali, 20 % sulfidity, and 7:1 liquid/solid ratio, according to Ibarra et al. [38]. The resulting cooked materials were filtered, and the black liquors were recovered. Kraft lignins were isolated from black liquors by acid precipitation (pH lowered to 2.5 with concentrated sulphuric acid), centrifuged and washed with acid water (pH 2.5), dried and finally homogenized.

2.3. Chemical composition and phenols content

The composition of the Kraft lignins was determined by using the Laboratory Analytical Procedures (LAP) for biomass analysis provided by the National Renewable Energies Laboratory standard analytical methods [39]. Thus, the samples were subjected to acid hydrolysis in two steps to determine the carbohydrate composition, being the hydrolysed liquids analyzed by high-performance liquid chromatography (1260 HPLC, Agilent, Waldbronn, Germany; fitted with a G1362A refractive index detector; and equipped with an Agilent Hi-PlexH). 5 mM sulphuric acid was pumped as mobile phase at 65 °C and 0.6 mL/min. The solid residues remaining after the acid hydrolysis were considered acid-insoluble lignin (Klason lignin). Acid-soluble lignin was determined in a UV–Visible spectrophotometer (Jasco V-500, Japan) at 205 nm.

The total phenols content of Kraft lignins was analyzed according to Jiménez-López et al. [6]. Kraft lignins were previously dissolved in dimethylsulfoxide (DMSO). Then, the absorbance of a mixture with Na_2CO_3, Folin-Ciocalteau reagent, and Kraft lignin solutions was measured at 760 nm using a UV–Vis spectrophotometer (Lambda 365, PerkinElmer, Boston, MA, USA). The total phenols content of samples was quantified using a calibration curve prepared from a standard solution of gallic acid (1–20 mg/L) and expressed as mg gallic acid equivalent (GAE)/g of lignin (on a dry basis).

2.4. Nuclear Magnetic Resonance (NMR)

^{13}C NMR experiments of Kraft lignins were carried out at 25 °C in a

Bruker AVANCE 500 MHz (Bruker, USA) spectrometer equipped with a 5 mm BBFO plus with a z-gradient double-resonance probe. Chemical shifts were referred to tetramethylsilane. DMSO was used as a solvent. ^{13}C NMR experiments were carried out under the following operation conditions: pulse 30° (μs) 3.21; recycle delay (s) 1; spectral width (Hz) 30,030; acquisition time (s) 1.09; scans number 12500 [40].

^{13}C—^{1}H two-dimensional Nuclear Magnetic Resonance (2D NMR) analysis of Kraft lignins (dissolved in 0.75 mL of deuterated dimethylsulfoxide, DMSO-d_6) was recorded at 25 °C in the same spectrometer. HSQC (heteronuclear single quantum correlation) experiment was recorded under the following operation conditions: spectral widths, 5000 Hz for the ^{1}H dimensions, and 22,522 Hz for ^{13}C dimensions; the number of collected complex points, 1024 for ^{1}H-dimension with a recycle delay of 1 s; scan number 32; time increments (^{13}C) 256; 1 JC-H (Hz): 145; *J*-coupling evolution delay set to 3.45 ms; squared cosine-bell apodization function applied in both dimensions. Residual DMSO (from DMSO-d_6) was used as an internal reference (δ_C/δ_H 39.6/2.5 ppm) [40].

2.5. Size Exclusion Chromatography (SEC)

SEC analysis of Kraft lignins was conducted on a HPLC (1260 HPLC, Agilent, Waldbronn, Germany, equipped with a G1362A refractive index (RI) detector and two columns PLgel 10 μm MIXED B 300 × 7.5 mm). DMF was pumped as mobile phase at the conditions described by Jiménez-López et al. [6]. Columns were calibrated with polystyrene standards (peak of average molecular weights of 570, 8900, 62,500, 554,000, Sigma-Aldrich, San Luis, MO, USA).

2.6. Fourier-transform infrared (FTIR) spectroscopy

FTIR spectra were performed using a JASCO FT/IR-4200 apparatus (Jasco Inc., Japan). The different Kraft lignins were dispersed in KBr to obtain disks with a diameter of 13 mm. Then, the disks are placed in a holder for measurements in wavenumber range from 400 to 4000 cm^{-1}, in transmission mode, at a resolution of 4 cm^{-1}.

2.7. Thermal analysis

Thermogravimetric analysis (TGA) of Kraft lignins and electrospun nanostructures were carried out under N_2 in an analyzer model Q-50 (TA Instruments, New Castle, USA). Samples (4 to 7 mg) were placed on platinum pans and heated from 25 °C to 600 °C, at 10 °C/min.

Differential scanning calorimetry (DSC) measurements of Kraft lignins and electrospun nanostructures were performed with a Q100 calorimeter (TA Instrument Waters, USA) by applying for a heating-cooling-heating program from 10 to 200 °C, at 10 °C/min, to eliminate the thermal history of the samples. Samples (5–10 mg) were placed in hermetically sealed aluminum pans. The sample was purged with nitrogen at a flow rate of 50 mL/min. Calibration of temperatures and enthalpy was performed with standard indium using the thermal software version 4.0. The glass transition temperatures were calculated from the calorimetric data obtained during the second heating ramp.

2.8. Electrospinning

The electrospun nanostructures were prepared based on previous studies. Thus, the electrospun lignin/cellulose acetate nanostructures were developed from solutions containing 20–30 wt% of eucalypt Kraft lignin and CA varying weight ratios from 100:0 to 60:40 in a DMF/Ac solution. Their morphology was found to be strongly dependent on the rheological properties of the biopolymer solution, and a synergy was found in the Kraft lignin:CA (70:30) system prepared at 30 wt%.

In this work, Kraft lignin/CA solutions in DMF/Ac (1:2 v/v) were manufactured at 30 wt% concentration using a Kraft lignin:CA weight ratio of 70:30. The solutions were prepared with a magnetic stirrer (500 rpm) at room temperature for 24 h.

The nanostructures were obtained through an electrospinning process using a vertical configuration. The processing conditions were: 20 cm between the aluminum collecting plate (cathode) and the needle tip (anode), a flow rate of 0.6 mL h^{-1} and a voltage of 17 kV. All experiments were performed at room temperature (22 ± 1 °C) and controlled relative humidity (45 ± 1 %).

2.9. Characterization of lignin/CA solutions

Kraft lignin/CA solutions were physicochemically characterized through surface tension, electrical conductivity measurements and shear viscosity. Surface tension measurements were performed using a platinum Wilhelmy plate at room temperature in a Sigma 703D (Biolint Science, Chine) force tensiometer. Electrical conductivity was measured in a CE GP31 high-frequency meter (Crison, Spain), where measurements were obtained through temporal stability. Shear viscosity was determined, at 25 °C, in an ARES controlled-strain rheometer (Rheometric Scientific, UK) using a Couette geometry at 25 °C in a shear rate range of 1–300 s^{-1}.

2.10. Characterization of electrospun nanostructures

The morphology of the electrospun nanostructures was evaluated using scanning electron microscopy (SEM) in a JXA-8200 SuperProbe (JEOL, Japan) operating at an acceleration voltage of 15 kV. Samples were previously gold-coated using a sputter coater HHV Scancoat Six SEM. [41]. The FIJI ImageJ analysis program was used to analyze the SEM images of the different systems. For each image of the system, 100 random measurements were made with the same magnification.

3. Results and discussion

3.1. Chemical composition of Kraft lignins

The resulting black liquors from Kraft pulping of poplar and OTP materials were acidified at pH 2.5 for lignin recovery. The composition of the precipitated lignins and the eucalypt industrial lignin is shown in Table 1. Eucalypt Kraft lignin sample showed the highest lignin content (total lignin of 98.2 %), followed by poplar (total lignin of 91.0 %) and OTP (total lignin of 72.0 %) Kraft lignins. Depending on the lignin reactivity during delignification processes, the lignin production from black liquors can vary. In this sense, the native lignin from OTP has been described as lignin with a low reactivity during delignification processes due to its relatively low S/G ratio and abundance of condensed (C—C linkages) substructures [42]. Contrary, eucalypt and poplar native lignins have displayed an abundance of S over G units together with a predominance of aryl-ether linkages [43,44], which makes these lignins more susceptible to delignification. It can explain the major quantities of lignins precipitated from Kraft black liquors of eucalypt and poplar compared to lignin from OTP. Nevertheless, the severity of pulping is another factor to consider [45].

Some carbohydrate impurities were determined in all lignins, being especially abundant in OTP lignin (12.2 % glucan, 9.3 % xylan and 1.0 % arabinan) compared to poplar (1.3 % glucan, 4.1 % xylan and 0.2 %

Table 1
Chemical composition of Kraft lignins.

	Composition (% dry weight)		
	Eucalypt	Poplar	OTP
Glucan	1.7 ± 0.05	1.3 ± 0.04	12.2 ± 0.05
Xylan	1.8 ± 0.03	4.1 ± 0.05	9.3 ± 0.06
Arabinan	–	0.2 ± 0.01	1.0 ± 0.05
Acid-soluble lignin	13.0 ± 0.1	6.9 ± 0.16	7.4 ± 0.22
Acid-insoluble lignin	85.2 ± 0.25	84.1 ± 0.07	64.6 ± 0.14
Total lignin	98.2	91.0	72.0

arabinan) and eucalypt (1.7 % glucan and 1.8 % xylan) lignins (Table 1). Part of these carbohydrates present in lignins come from their solubilization during alkaline pulping, which starts rapidly when the lignocellulosic fibers come in contact with the alkaline pulping liquor [45]. Their solubilization depends significantly on cooking severity, proceeding rapidly at temperatures close to 100 °C for the xylans and at temperatures about 170 °C, or higher, for glycosidic bonds [45]. Subsequently, these solubilized carbohydrates can partly precipitate during lignin isolation due to their lower solubility under acidic conditions, explaining the carbohydrates impurities content determined in Kraft lignin samples [46]. Nevertheless, the carbohydrate contamination can also be attributed to lignin-carbohydrate complexes [47]. Similar results have been previously reported in lignins recovered by precipitation from alkaline black liquors, i.e., Kraft and soda, of eucalypt, poplar and OTP materials [48–50].

3.2. 2D NMR spectra analysis of Kraft lignins

The 2D NMR HSQC spectra of Kraft lignins are displayed, including the whole spectra (δ_C/δ_H 0.0–150.0/0.0–9.0) in supplementary Fig. 1S and the spectra corresponding to the oxygenated aliphatic (δ_C/δ_H 45.0–95.0/2.5–6.0 ppm) and the aromatic (δ_C/δ_H 90.0–150.0/5.0–9.0 ppm) regions in Figs. 1 and 2, respectively. The main $^{13}C—^{1}H$ lignin correlation signals identified in HSQC spectra are shown in Table 2, attributed according to those reported by different studies [42,48,49,51–60]. The lignin substructures and carbohydrates identified are depicted in Figs. 3 and 4.

The non-oxygenated aliphatic region (around δ_C/δ_H 0.0–50.0/0.0–5.0 ppm) of the different Kraft lignin spectra showed a diversity of saturated aliphatic moieties (Fig. 1S), including signals that some studies have associated to extractives [61]. Other studies have attributed these signals to lignin depolymerization such as oxygen-containing groups, e.g., alcohol, carbonyl and ethers and groups, neighbouring alkene [48].

The oxygenated aliphatic region of Kraft lignin spectra showed information about the different inter-unit linkages present in these lignins (Fig. 1), including those from native and Kraft-derived linkages. Despite the well-known β-O-4′ linkage breakdown under alkaline conditions during Kraft or soda pulping processes [48,56,59], several remaining signals from native β-O-4′ substructures (C_α–H_α for β-O-4′ G and S lignin units (A_α), C_β–H_β for β-O-4′ S units (A_β), and C_γ–H_γ (A_γ)) could still be observed in the oxygenated aliphatic region of all spectra, being more noticeable in eucalypt lignin (Fig. 1a) compared to poplar and OTP lignins (Figs. 1b and c, respectively). Nevertheless, as a result of β-O-4′ linkage degradation, high phenolic content was observed by ^{13}C NMR for all kraft lignin samples, showing a predominance of phenolic units (C_3 and C_5 of phenolic S units at δ_C 147 ppm) compared to non-phenolic units (C_3 and C_5 of etherified S units at δ_C 153 ppm and C_1 of etherified S units at δ_C 135 ppm) (Fig. 2S) [62]. These results are in concordance with the total phenols content measured with Folin-Ciocalteau reagent, showing the highest values for eucalypt Kraft lignin (627.43 ± 0.345 mg GAE/g lignin) followed by poplar Kraft lignin (585.72 ± 0.241 mg GAE/g lignin) and OTP Kraft lignin (295.42 ± 0.062 mg GAE/g lignin). C_β–H_β correlation (C_β) from native β-5′ phenylcoumaran substructures was also observed in eucalypt Kraft lignin (Fig. 1a), whereas C_γ–H_γ correlation (C_γ) was also detected in poplar and OTP Kraft lignin spectra (Fig. 1b and c, respectively). Phenylcoumaran substructure is also susceptible to be degraded under alkaline conditions during Kraft or soda pulping processes [56,59]. On the other hand, the predominant signals corresponding to native lignin linkages found in all lignin spectra were assigned to β-β′ resinol substructures, including correlations of C_α–H_α (B_α), C_β–H_β (B_β) and the double C_γ–H_γ (B_γ). This resinol substructure with C—C bonds is generally more stable to alkaline pulping conditions of Kraft or soda pulping processes than β-O-4′ and β-5′ phenylcoumaran substructures [54,59]. Finally, other signals from native lignin linkages were also visible. Then, C_α–H_α (E_α) and $C_{\alpha'}$–$H_{\alpha'}$ ($E_{\alpha'}$) correlations for

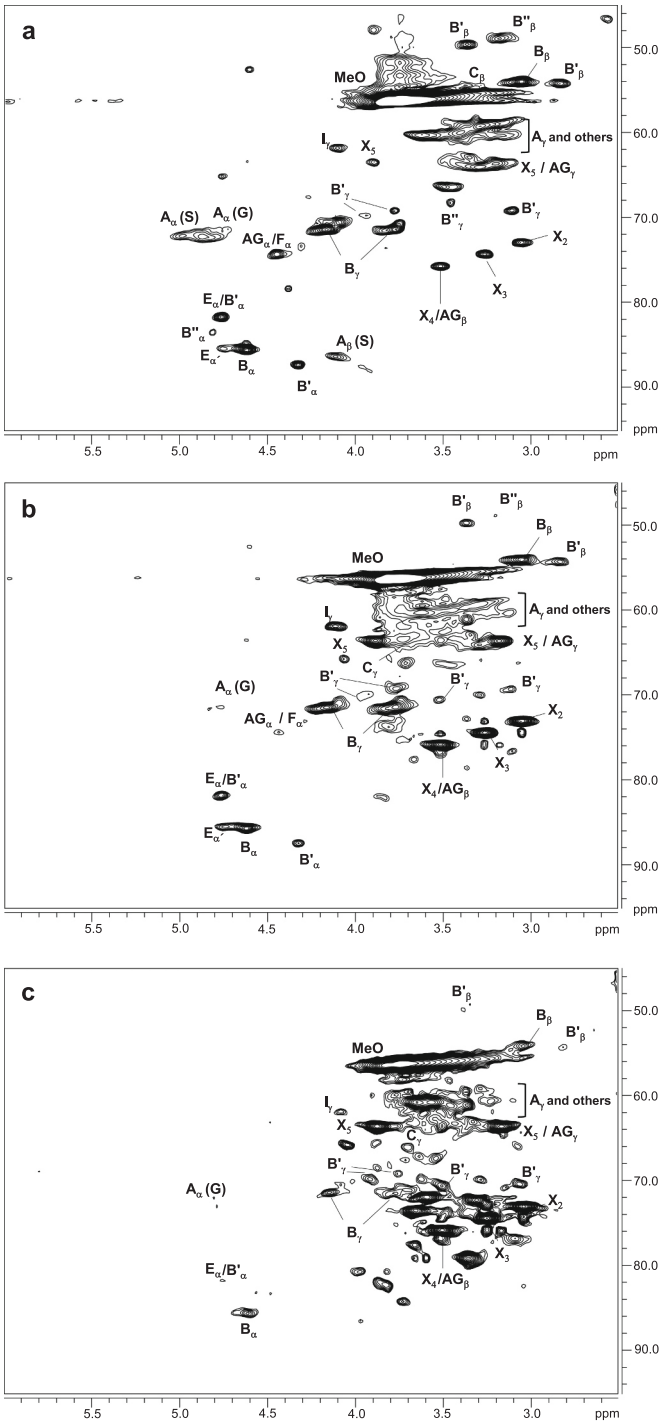

Fig. 1. HSQC 2D-NMR spectra, δ_C/δ_H 45.0–95.0/2.5–6.0 ppm aliphatic oxygenated region, of eucalypt (a), poplar (b), and OTP (c) Kraft lignins.

spirodienones and C_γ–H_γ correlation for cinnamyl alcohol end-groups (I_γ) were detected in all lignin spectra (Fig. 1).

Signals from Kraft-derived lignin linkages could also be identified in the oxygenated aliphatic region of all spectra (Fig. 1). Among them, signals from episresinols (B′) and diaresinol (B″), both diastereomers resulting from the transformation of native resinol substructure during Kraft pulping [55,60], were observed in all lignins. These signals included C_α–H_α (B'_α), C_β–H_β (B'_β) and C_γ–H_γ (B'_γ) correlations from episresinols in all lignin spectra, together with C_α–H_α (B''_α), C_β–H_β (B''_β) and C_γ–H_γ (B''_γ) correlations from diaresinol in the case of eucalypt Kraft lignin (Fig. 1a). Aryl-glycerol substructure (AG), with correlations of

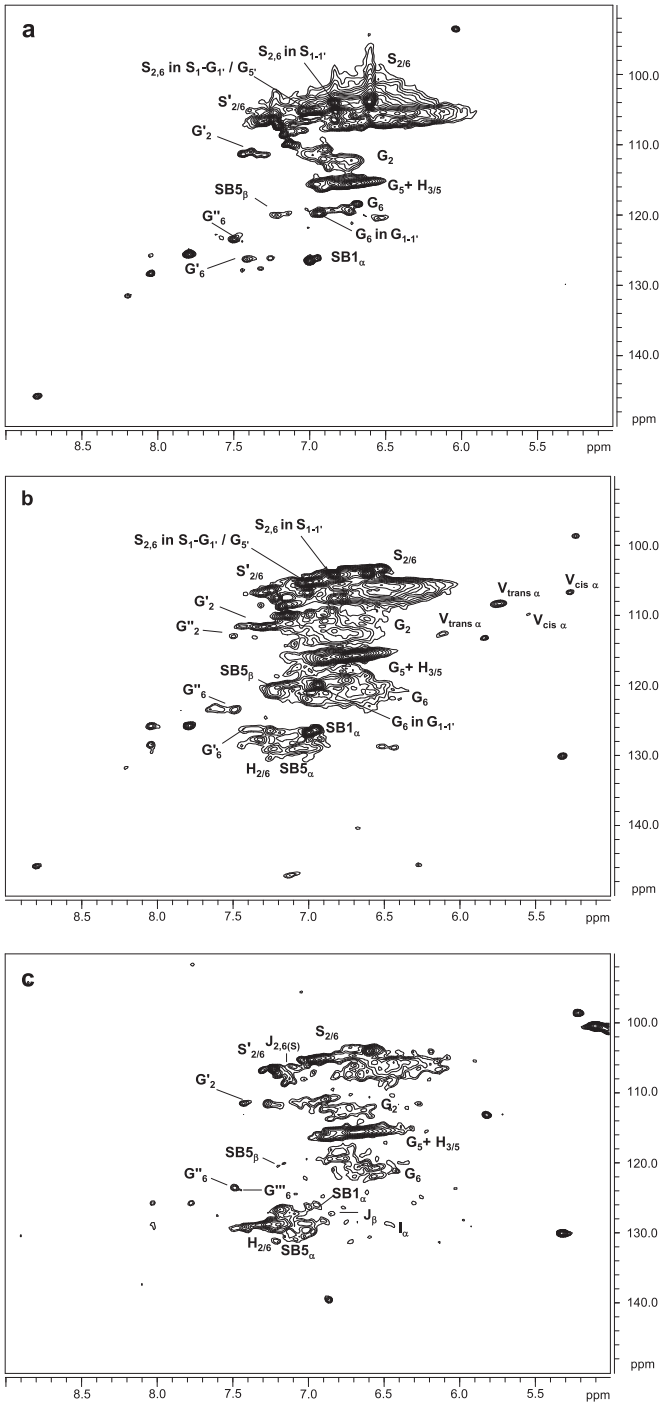

Fig. 2. HSQC 2D-NMR spectra, δ_C/δ_H 90.0–150.0/5.0–9.0 ppm aromatic region, of eucalypt (a), poplar (b), and OTP (c) Kraft lignins.

C_α–H_α (AG_α), C_β–H_β (AG_β) and C_γ–H_γ (AG_γ), could be hesitantly identified in eucalypt and poplar lignin spectra (Fig. 1a and b, respectively), and C_β–H_β and C_γ–H_γ in the case of OTP lignin (Fig. 1c). Aryl-glycerol substructure is produced from the non-phenolic β-aryl ether linkage under alkaline conditions during Kraft or soda pulping processes [59]. Finally, C_α–H_α correlation signal of lignin terminal structures with a carboxyl group in C_β (Ar-CHOH-COOH; F_α), overlapping with C_α–H_α correlation signal of aryl-glycerol substructure, could also be observed in eucalypt and poplar Kraft lignin spectra (Fig. 1a and b, respectively). This type of lignin terminal structures has previously been reported during Kraft pulping of elm, poplar and spruce [49,51,59].

Table 2
Assignment of main lignin and carbohydrates ^{13}C—^{1}H correlation signals in the HSQC spectra of Kraft lignins.

δ_C/δ_H (ppm)	Assignment
48.9/3.18	C_β–H_β, diaresinol substructures (**B″**)
49.6/3.36	C_β–H_β, episresinol substructures (**B′**)
54.0/2.83	C_β–H_β, episresinol substructures (**B′**)
53.9/3.05	C_β–H_β, resinol substructures (**B**)
54.3/3.38	C_β–H_β, phenylcoumaran substructures (**C**)
56.1/3.72	C–H, methoxyls (**MeO**)
60.6/3.40–3.64	C_γ–H_γ, β-O-4′ substructures (**A**)
61.8/4.11	C_γ–H_γ, cinnamyl alcohol end groups (**I**)
62.4/3.69	C_γ–H_γ, phenylcoumaran substructures (**C**)
63.4/3.23–3.89	C_5–H_5, xylan
63.6/3.11	C_γ–H_γ, aryl-glycerol (**AG**)
68.2/3.45	C_γ–H_γ, diaresinol substructures (**B″**)
69.3/3.30–3.71	C_γ–H_γ, episresinol substructures (**B′**)
70.2/3.73–4.10	C_γ–H_γ, episresinol substructures (**B′**)
71.4/3.77–4.17	C_γ–H_γ, resinol substructures (**B**)
71.8/4.86	C_α–H_α, β-O-4′ **G** unit (**A**)
72.3/4.88	C_α–H_α, β-O-4′ **S** unit (**A**)
73.0/3.09	C_2–H_2, xylan
74.0/4.42	C_α–H_α, aryl-glycerol (**AG**)
74.3/3.30	C_3–H_3, xylan
74.3/4.44	C_α–H_α, Ar–CHOH–COOH units (**F**)
75.6/3.48	C_β–H_β, aryl-glycerol (**AG**)
75.9/3.53	C_4–H_4, xylan
81.7/4.75	C_α–H_α, spirodienone substructures (**E**)
81.9/4.76	C_α–H_α, episresinol substructures (**B′**)
83.5/4.80	C_α–H_α, diaresinol substructures (**B″**)
85.5/4.77	$C_{\alpha'}$ –$H_{\alpha'}$, spirodienone substructures (**E**)
85.5/4.63	C_α–H_α, resinol substructures (**B**)
86.3/4.10	C_β–H_β, β-O-4′ **S** unit (**A**)
87.6/4.31	C_α–H_α, episresinol substructures (**B′**)
101.9/4.31	C-1, (1–4) β-D-Xylp
104.1/6.62	$C_{2,6}$–$H_{2,6}$, S units (**S**)
103.9/6.84	$C_{2,6}$–$H_{2,6}$, 3,5-tetramethoxy-*para*-diphenol substructures (**$S_{1\text{-}1'}$**)
105.0/6.9	$C_{2,6}$–$H_{2,6}$, **S_1-$G_{1'}$/$G_{5'}$** substructures
106.2/7.12	$C_{2,6}$–$H_{2,6}$, cinnamaldehyde end-groups (**J**)
106.6/5.27	C_α–H_α, isomer cis of vinyl ether (**V**) in **S**–**S**
107.0/7.31	$C_{2,6}$–$H_{2,6}$, oxidized (H–C_α = O or H_3C–C_α = O) S units (**S′**)
108.1/5.74	C_α–H_α, isomer trans of vinyl ether (**V**) in **S**–**S**
109.8/5.55	C_α–H_α, isomer cis of vinyl ether (**V**) in **S**–**G**
110.0/7.15	C_2–H_2, 3-dimethoxy-*para*-diphenol substructures (**$G_{1\text{-}1'}$**)
110.8/6.90	C_2–H_2, G units (**G**)
111.3/7.39	C_2–H_2, oxidized (H–C_α = O) G units (**G′**)
112.6/6.11	C_α–H_α, isomer trans of vinyl ether (**V**) in **S**–**G**
112.9/7.49	C_2–H_2, oxidized (H_3C–C_α = O) G units (**G″**)
115.0/6.74	$C_{3,5}$–$H_{3,5}$, *p*-hydroxyphenyl (**H**)
115.1/6.41–6.80	C_5–H_5, G units (**G**)
119.6/6.78	C_6–H_6, G units (**G**)
119.8/6.96	C_6–H_6, 3-dimethoxy-*para*-diphenol substructures (**$G_{1\text{-}1'}$**)
120.3/7.25	C_β–H_β, stilbene (**$SB5_\beta$**)
123.5/7.51	C_6–H_6, oxidized (H_3C–C_α = O) G units (**G″**)
123.8/7.49	C_6–H_6, oxidized (HO–C_α = O) G units (**G‴**)
126.4/6.99	C_α–H_α, stilbene (**$SB1_\alpha$**)
126.6/6.76	C_β–H_β, cinnamaldehyde end-groups (**J**)
126.8/7.42	C_6–H_6, oxidized (H–C_α = O) G units (**G′**)
128.3/6.45	C_α–H_α, cinnamyl alcohol end groups (**I**)
128.4/7.15	$C_{2,6}$–$H_{2,6}$, *p*-hydroxyphenyl (**H**)
128.8/7.11	C_α–H_α, stilbene (**$SB5_\alpha$**)

According to the chemical composition of Kraft lignins (Section 2.1), carbohydrate signals, either from hexose or pentose units, were also shown in the oxygenated aliphatic region of all spectra (Fig. 1), being particularly intense in OTP lignin (Fig. 1c). Among pentose units, signals correlations of xylan chain for C_2–H_2 (X_2), C_3–H_3 (X_3), C_4–H_4 (X_4), and C_5–H_5 (X_5) were clearly visible in all spectra, together with the C-1 cross peak for (1–4) β-D-Xylp of xylan (Fig. 1S).

The aromatic region of Kraft lignin spectra showed the typical correlation signals of S, G, and H lignin units (Fig. 2), the characteristic pattern of lignin from hardwood [42]. The S lignin units showed correlation signals of $C_{2,6}$–$H_{2,6}$ ($S_{2,6}$); whereas the G lignin units displayed correlation signals for C_2–H_2 (G_2), C_5–H_5 (G_5), and C_6–H_6 (G_6); and the H lignin units showed correlation signals of $C_{2,6}$–$H_{2,6}$ ($H_{2,6}$) and

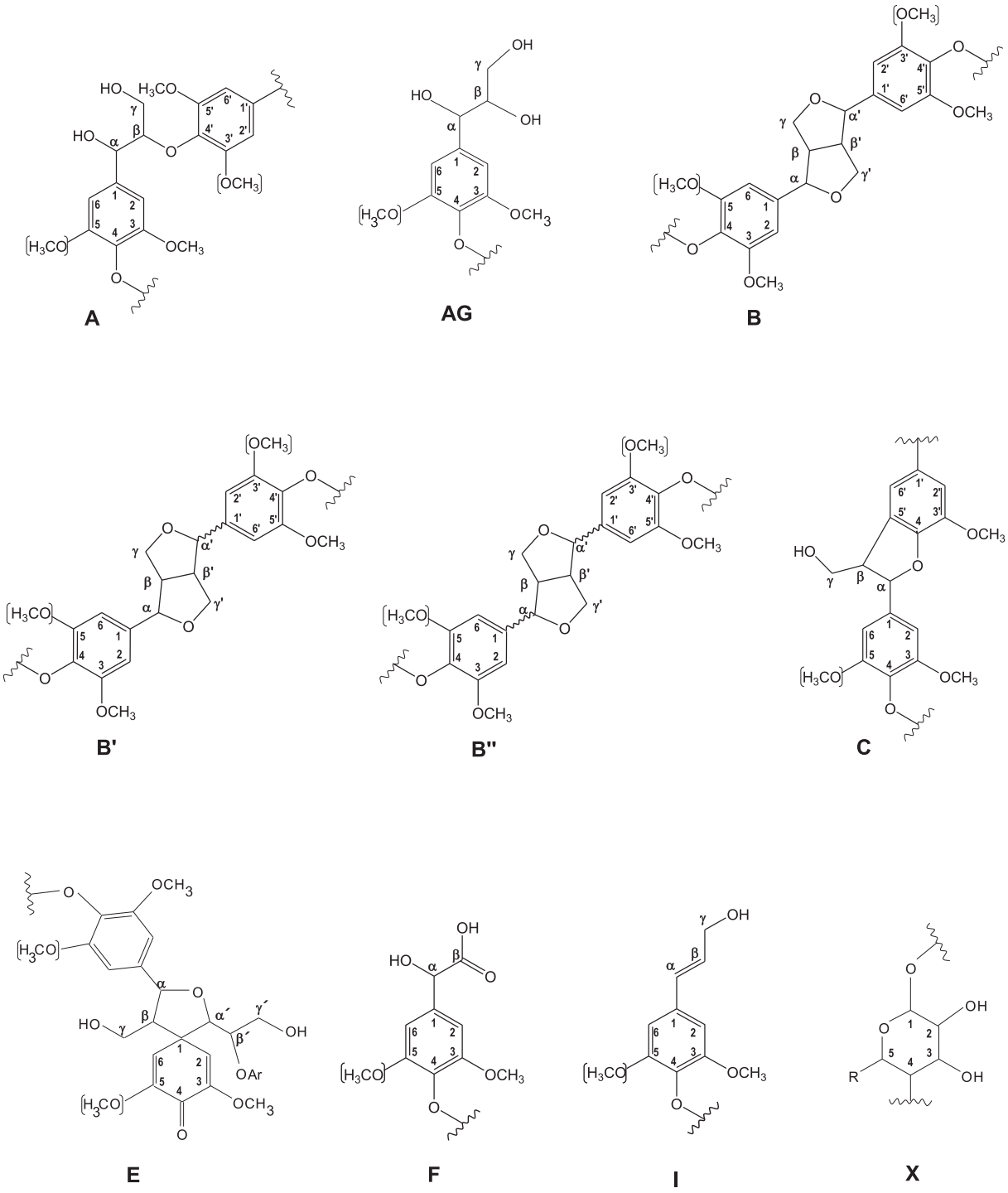

Fig. 3. Main lignin and carbohydrate substructures identified in aliphatic oxygenated region of eucalypt, poplar, and OTP Kraft lignins: **A**, β-*O*-4′ alkyl-aryl ether; **AG**, aryl-glycerol; **B**, resinols; **B′**, epiresinol; **B″**, diaresinol; **C**, phenylcoumarans; **E**, spirodienones; **F,** Ar–CHOH–COOH; **I**, cinnamyl alcohol end-groups; **X**, xylopyranose (R, OH).

$C_{3,5}$–$H_{3,5}$ ($H_{3,5}$). In addition, a group of signals from alkaline-catalyzed oxidation of aromatic side-chains of lignin could also be detected in all Kraft lignin spectra. Among them, $C_{2,6}$–$H_{2,6}$ in oxidized S units ($S'_{2,6}$) with an aldehyde end-group (syringaldehyde) or ketone end-group (acetosyringone) in C_α; and signals from oxidized G units, including correlations endorsed to C_2–H_2 (G'_2) and C_6–H_6 (G'_6) in C_α oxidized G units with an aldehyde end-group (vanillin), C_2–H_2 (G''_2) and C_6–H_6 (G''_6) in C_α oxidized G units with a ketone end-group (acetovanillone), and C_6–H_6 (G'''_6) in C_α oxidized G units with a carboxylic end-group (vanillic acid). In this sense, Prinsen et al. [56] and Zhao et al. [60] reported a high lignin oxidation, with a variety of aldehyde, ketone and carboxylic end-groups during alkaline pulping processes, i.e., Kraft and soda, of eucalypt. Finally, other native lignin units corresponding to C_β–H_β (J_β) and $C_{2,6}$–$H_{2,6}$ ($J_{2,6}$) of cinnamaldehyde end-groups and C_α–H_α (I_α) of cinnamyl alcohol end-groups could be identified in the aromatic region of olive Kraft lignin spectrum (Fig. 2c).

Signals from Kraft-derived lignin linkages were also observed in the aromatic region of all lignin spectra. Correlation signals endorsed to

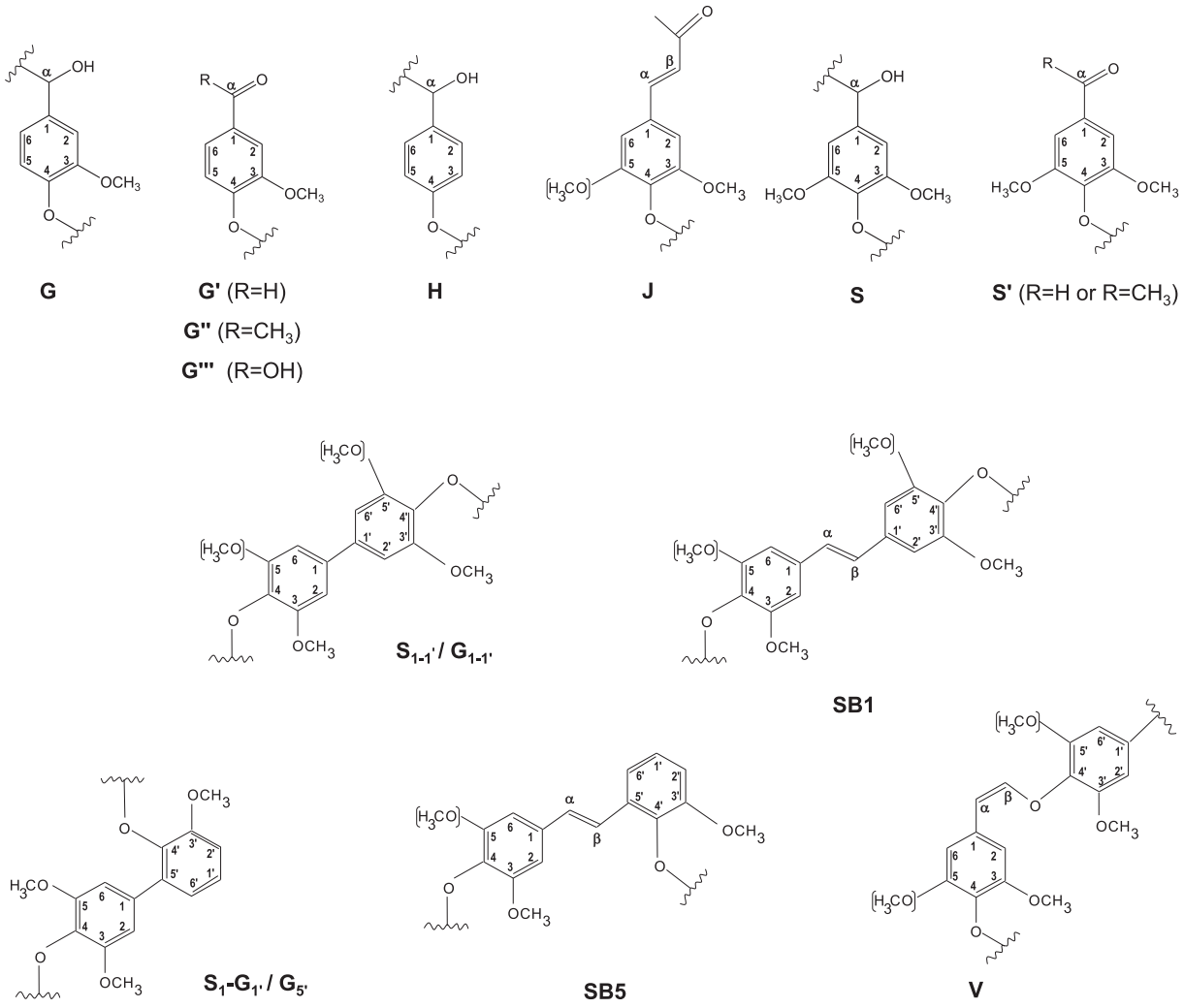

Fig. 4. Main lignin substructures identified in aromatic region of eucalypt, poplar, and OTP Kraft lignins: **G**, guaiacyl unit; **G′**, vanillin; **G″**, acetovanillone; **G‴**, vanillic acid; **H**, *p*-hydroxyphenyl unit; **J**, cinnamyl aldehyde end-groups; **S**, syringyl unit; **S′**, syringaldehyde; **S″**, acetosyringone; **$S_{1\text{-}1'}$**, 3,5-tetramethoxy-*para*-diphenol; **$G_{1\text{-}1'}$**, 3-dimethoxy-*para*-diphenol; **S_1-$G_{1'}$/$G_{5'}$**; **SB1,** stilbene-β-1′; **SB5,** stilbene-β-5′;**V**, vinyl ether.

C_α–H_α in β1 stilbene ($SB1_\alpha$) and C_α–H_α and C_β–H_β in β5 stilbene ($SB5_\alpha$ and $SB5_\beta$, respectively) were identified in all lignin samples. β1 stilbene has been described as a degradation product from spirodienone, whereas β5 stilbene from β-5′ phenylcoumaran, both via reversed aldol addition during alkaline pulping processes, i.e., Kraft and soda, of eucalypt and spruce [53,55]. On the other hand, correlation signals associated to C_α–H_α in vinyl-ether were also observed in poplar Kraft lignin spectrum (Fig. 2b), including correlations from their corresponding two isomers (V_{trans} and V_{cis}), comprising different combinations of G and S units (V(G–G), V(S–G), V(G–S) and V(S–S)) [60]. Vinyl-ether is usually formed from β-O-4′ substructures with free phenolic hydroxyls under alkaline pulping processes, i.e., Kraft and soda processes, via reversed aldol addition, being reported in solubilized lignins during Kraft and soda pulping from elm, eucalypt and spruce [50,59,60]. Finally, correlation signals for $S_{2,6}$ in $S_{1\text{-}1'}$ (3,5-tetramethoxy-para-diphenol), G_2 and G_6 in $G_{1\text{-}1'}$ (3-dimethoxy-para-diphenol) and $S_{2,6}$ in S_1_$G_{1'}$/$G_{5'}$ were tentatively identified in eucalypt and poplar Kraft lignin spectra (Fig. 2a and b, respectively). These structures have been recently described in eucalypt, spruce and elm lignins during Kraft pulping as a result of C_α-C_1 breakdown in a retro-aldol reaction, followed by radical coupling reaction [51–53].

Quantification of the abundance of the main lignin substructures and end-groups (per 100 aromatic units), as well as the abundance of the aromatic units (molar percentage) and S/G ratios, present in the different Kraft lignins, was performed by the integration of the volume contours of their correlation signals (see Table 3). As previously commented, the β-O-4′ alkyl-aryl ether linkages breakdown is the principal way for lignin depolymerization under alkaline pulping conditions, i.e., Kraft and soda processes, producing soluble low molecular weight aromatic fragments with high phenolic content [56,59]. C—C linkages from phenylcoumaran (β-5′) can also be fragmented under alkaline conditions, whereas from resinol (β-β′) are generally more stable [56,59]. According to this, Kraft lignins from poplar and OTP exhibited a higher content of β-β′ resinol (4.4 linkages per 100 aromatic units) and β-5′phenylcoumaran (2.7 and 5.3 linkages per 100 aromatic units for poplar and OTP lignins, respectively) substructures compared to β-O-4′ alkyl-aryl ether (1.8 linkages per 100 aromatic units for poplar lignin; and 0.3 linkages per 100 aromatic units for OTP lignin). In the case of eucalypt Kraft lignin, a slightly higher content of β-O-4′ (5.9 linkages per 100 aromatic units) than that β-β′ resinol (4.6 linkages per 100 aromatic units) was quantified. In this sense, Prinsen et al. [56] reported a higher abundance of β-β′ resinol substructures together with a limited or null abundance of both β-O-4′ and β-5′ phenylcoumaran substructures when eucalypt was subjected to Kraft pulping. In the same line, similar trend has also been described by Martín-Sampedro et al. [49] during Kraft pulping of poplar and by Eugenio et al. [50] during soda pulping of OTP material. Spirodienone (1.8, 1.6 and 0.6 linkages per 100 aromatic units for eucalypt, poplar and OTP lignins, respectively), aryl-glycerol (1.4

Table 3
Abundance of lignin substructures and end-groups (per 100 aromatic units) and aromatic units (molar percentage) from integration of $^{13}C—^{1}H$ correlation signals in the HSQC spectra of Kraft lignins.

	Eucalypt	Poplar	OTP
β-O-4′ (**A**)	5.9	1.8	0.3
Resinols (**B**)	4.6	4.4	4.4
Phenylcoumarans (**C**)	–	2.7	5.3
Spirodienones (**E**)	1.8	1.6	0.6
Arylglicerol (**AG**)	1.4	0.6	–
Ar-CHOH-COOH (**F**)	1.4	0.6	–
cinnamyl alcohol end-groups (**I**)	1.0	0.4	2.0
cinnamaldehyde end-groups (**J**)	–	–	1.4
Stilbene (**SB1**)	2.1	6.5	4.2
Stilbene (**SB5**)	0.6	4.1	6.7
Vinyl-ether (**V**)	–	3.2	–
H (%)	–	0.7	4.0
G (%)	11.2	17.5	27.3
S (%)	88.8	81.4	68.7
S/G ratio	7.9	4.7	2.5

Abundance of β-O-4′, resinols, spirodienones, arylglicerol and Ar-CHOH-COOH substructures was estimated by 2D-NMR from C_α–H_α correlations. Cinnamyl alcohol end-groups and phenylcoumarans using C_γ–H_γ correlations; Cinnamaldehyde end-groups using C_β–H_β correlations; Vinyl-ether and stilbenes (SB1 and SB5) using C_α–H_α correlations; $C_{2,6}$–$H_{2,6}$ correlations from S units; and C_2–H_2 correlations from G units were used to estimate the S/G lignin ratios.

linkages per 100 aromatic units for eucalypt lignin and 0.6 linkages per 100 aromatic units for poplar lignin) and Ar-CHOH-COOH (1.4 and 0.6 linkages per 100 aromatic units for eucalypt and poplar lignins, respectively) substructures were quantified. Nonetheless, the abundances quantified for Ar-CHOH-COOH and spirodienones substructures could be overestimated by the overlay of their signals with those from aryl-glycerol and epiresinols, respectively. Finally, cinnamyl alcohol end-groups were also quantified (2.0, 1.0 and 0.4 linkages per 100 aromatic units for OTP, eucalypt and poplar lignins, respectively) together with cinnamaldehyde end-groups in OTP lignin (1.4 linkages per 100 aromatic units).

Regarding the S/G ratio, all Kraft lignins showed a high abundance of S lignin units, especially for eucalypt and poplar lignins (7.9 and 4.7, respectively) compared to OTP lignin (2.5). It is well-known the preferential solubilization of S lignin units, which are mostly forming β-O-4′ alkyl-aryl ether in hardwoods [43], during alkaline pulping processes i.e., Kraft and soda processes, of eucalypt, poplar and OTP materials [49,56]. Thus, OTP native lignin shows a lower reactivity to delignification due to its low S/G ratio and abundance of C—C linkages, compared to eucalypt and poplar native lignins. Moreover, the lower S/G of OTP native lignin may also explain the lower S/G ratio observed for OTP Kraft lignin compared to eucalypt and poplar Kraft lignins. The abundance of stilbene substructures were also quantified in all lignins, displaying higher quantities in poplar (6.5 and 4.2 linkages per 100 aromatic units for stilbene-β1 and stilbene-β5, respectively) and OTP lignins (4.1 linkages per 100 aromatic units for stilbene-β1 and 6.7 linkages per 100 aromatic units for stilbene-β5) compared to eucalypt lignin (2.1 and 0.6 linkages per 100 aromatic units for stilbene-β1 and stilbene-β5, respectively). Finally, vinyl-ether were quantified in poplar Kraft lignin (3.2 linkages per 100 aromatic units), whereas cinnamaldehyde end-groups were measured in OTP Kraft lignin (1.4 linkages per 100 aromatic units).

3.3. SEC analysis of Kraft lignins

The molecular weight distributions of Kraft lignins are displayed in Fig. 3S. From them, weight-average (Mw) and number-average (Mn) molecular weights, as well as polydispersity (Mw/Mn) values were calculated (Table 4). The low molecular weight values of lignins (5.3 KDa, 5.4 KDa and 4.8 KDa for eucalypt, poplar and OTP lignins, respectively) clearly revealed the high degradation of the lignin

Table 4
Weight average (*Mw*) and number-average (*Mn*) molecular weights and polidispersity (*Mw/Mn*) of Kraft lignins. Mw and Mn are given in Da.

	Kraft lignins		
	Eucalypt	Poplar	OTP
Mw	5285	5445	4780
Mn	4230	4550	4390
Mw/Mn	1.24	1.19	1.08

macromolecule during the Kraft pulping process. This fact corroborates the preferential breakdown of β-O-4′ alkyl-aryl ether linkages previously showed by 2D NMR as well as the high phenolic content observed by ^{13}C NMR (Section 3.2). In this sense, Prinsen et al. [56] already reported an important decrease in the molecular weight values of eucalypt lignin due to a strong cleavage of β-O-4′ alkyl-aryl ether linkages produced during alkaline pulping processes such as Kraft and soda. Similarly, Martín-Sampedro et al. [49] described low molecular weight values together with an extended breakdown of β-O-4′ alkyl-aryl ether linkages in lignin from poplar during Kraft pulping, and Eugenio et al. [50] in lignin from OTP during soda pulping. Furthermore, the low molecular weight lignin fragments resulting from depolymerization of the lignin macromolecule during Kraft pulping were also uniformly distributed, as low polydispersity values reflected (Table 4).

3.4. Fourier-transform infrared (FTIR) spectroscopy of Kraft lignins

Fig. 4S shows the FTIR spectra of the Kraft lignins studied. The corresponding bands were assigned in comparison with other previously reported lignin spectra [40,63–65]. All spectra displayed a broad band at 3400 cm^{-1} associated with O—H stretching vibration in the aromatic and aliphatic lignin structures. On the other hand, the corresponding asymmetric and symmetric stretching vibrations of the methylene groups are observed at 2939 and 2834 cm^{-1}, respectively. In accordance with the chemical composition shown above, the FTIR spectra display the typical bands of lignin, which include those found at 1612, 1515 and 1415 cm^{-1} related to the vibrations of the aromatic skeleton. Other bands correspond to syringyl (S) and guaiacyl (G) units, at 1315 cm^{-1} (aromatic ring breathing, S and G condensed units), 1268 cm^{-1} (G ring breathing with C═O stretching), 1218 cm^{-1} (G ring breathing with C—C, C—O, and C═O stretching), 1115 cm^{-1} (C—H bond deformation in S units), and 818 cm^{-1} (C—H out of plane deformation of S units). Regarding the presence of carbohydrates, different bands associated with cellulose and hemicelluloses were detected in the OTP Kraft lignin, in agreement with the chemical composition of this lignin. Thus, a carbohydrate region with bands characteristic of cellulose and hemicelluloses is evidenced at 1156, 1115 and 1026 cm^{-1} (C—O asymmetric vibration, C-OH skeletal vibration and C—O stretching vibration, respectively). This region could also be overlapped by a broad band at 1114 cm^{-1} related to the asymmetric stretching of $SO_4^{=}$ groups, resulting from the salts generated during the acid precipitation for lignin recovery from Kraft black liquors. On the other hand, the band at 1715 cm^{-1}, more intense in OTP, is attributed to the carbonyl groups of hemicellulose according to its higher xylose content or an unconjugated C═O stretching, as a consequence of the lignin oxidation [46], supporting the observations displayed by 2D NMR (Section 3.2).

3.5. Thermal analysis of Kraft lignins

In general, the thermal behavior of a polymer is highly related to its molecular weight and chemical structure. The thermal properties of Kraft lignins (eucalypt, poplar and OTP) were investigated by TGA and DSC. Figs. 5a and b show weight loss (TG) and weight loss derivative function (DTG) versus temperature, respectively. All lignin thermograms were in accordance with other works reported in the literature [65,66]. The onset temperature for thermally-induced weight loss

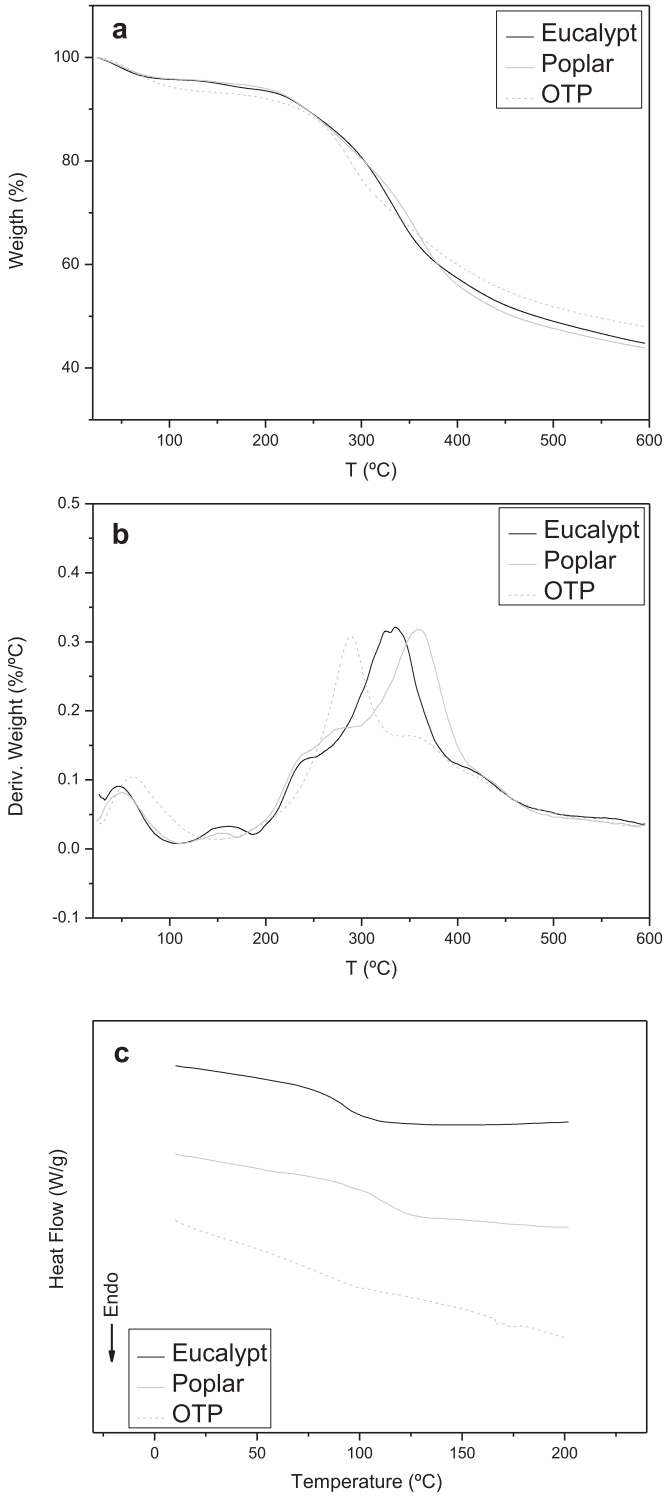

Fig. 5. TGA curves in the form of weight loss (a) and its derived function (b) versus temperature for eucalypt (black continuous line), poplar (gray continuous line) and OTP (gray discontinuous line) Kraft lignins. DSC curves (c) for eucalypt (black continuous line), poplar (gray continuous line) and OTP (gray discontinuous line) Kraft lignins.

(T_{onset}), the maximum weight-loss rate temperature (T_{max}), the weight loss at the end of each decomposition step and the percentage of non-degraded residue were calculated from the thermogram of each sample studied (Table 5). All lignin samples exhibited different weight loss stages [65]. The initial thermal degradation around 50–70 °C for Kraft lignin samples is attributed to the weight loss of moisture (4–6 %). Later on, at T_{max} of 141–143 °C for eucalypt and poplar, the small weight losses are a consequence of both residual hemicellulose [67] and dehydration of hydroxyl groups present on lignin structure [68]. On the other hand, one of the main weight losses is achieved around 241–359 °C, assigned to the cleavage of β-O-4 linkages, what is due to its low thermal stability at temperatures below 350 °C [65], leading to the formation of many volatile groups at these temperatures such as guaiacol, dimethoxyphenol, dimethoxyacetophenone and trimethoxyacetophenone. Overlapped to this weight loss and generally comprising a unique combined event, the β-aryl–alkyl–ether linkages scission (200–300 °C) are found, as well as the rupture of the aliphatic side chains joined to the aromatic units. The decomposition of aromatic rings and C—C cleavage of lignin structural units occurs at higher temperatures (418–437 °C) [68,69,70,71]. Further, a continuous decrease up to a final residue at around 44–48 % is dependent on the selected biomass. These results revealed that all lignins are stable at high temperatures which are associated with the high degree of branching and formation of highly condensed aromatic structures. The thermal stability of lignins depends on their structure (functional groups and linkages), on their molecular weight and, therefore, on the origin and the extraction processes applied, which determine the chemical composition of each sample [72]. Thus, poplar lignin exhibits higher thermal stability because it has a slightly higher molecular weight related with its higher aryl-ether substructures content. Whereas, OTP lignin presents a lower thermal decomposition rate and broader thermal decomposition region due to the presence of more carbohydrates and lower molecular weight associated with its lower aryl-ether substructures content. Regarding the high residue percentages existing in the Kraft lignins, it can be attributed to the presence of ashes probably related to the inorganic compounds used in Kraft pulping (e.g., NaOH and Na_2S), the high amount of Na_2SO_4 salts formed during the acid lignin precipitation step, and the inorganic compounds present in raw material. In the case of OTP lignin, the highest residue percentage observed (48 %), compared to eucalypt and poplar lignins (44–45 %), could be due to the higher content of inorganic compounds in the OTP raw material. Generally, the high amount of ash content in OTP material appears due to the existence of leaves together the soil contamination that is unavoidable in mechanized harvesting [73]. Moreover, the higher content of salts generated during acid OTP lignin precipitation (observed previously by FTIR analysis) could also contribute to these ashes.

Table 5
TGA characteristics parameters and glass transition of Kraft lignins.

Kraft lignins	T_{onset} (°C)	T_{max} (°C)	Weight loss (%)	Residue (%)	T_g (°C)
Eucalypt	143/269	157/241/335/418	2/49	45	92
Poplar	141/279	151/271/359/437	1/50	44	110
OTP	252/417	289/352/424	19/27	48	87

Fig. 5c shows the DSC thermograms of different Kraft lignins (eucalypt, poplar and OTP) during the second heating cycle. The thermal event distinguished in the DSC thermograms can be assigned to the glass transition (T_g) of each lignin, which is listed in Table 5. The T_g of lignin is affected by several factors, such as molecular weight, thermal history, and degree of cross-linking [74]. As can be seen, poplar lignin has the highest T_g (110 °C), followed by eucalypt lignin (92 °C) and, finally, OTP lignin (87 °C). This is in accordance with the previously discussed molecular weight results. The high molecular weight of lignin suggests that it contains few chains ends resulting in low volume mobility, thus more energy is required to rotate the chain [75]. Therefore, there is a correlation of the T_g values with molecular weight obtained from Kraft lignins as reported by Hu et al. [76].

3.6. Physicochemical properties of Kraft lignin/CA solutions

Intrinsic properties of Kraft lignin/CA solutions, mainly surface tension, electrical conductivity, and viscosity can affect the electrospinnability and morphology of electrospun nanostructures [27,32–34]. These properties are listed in Table 6 for the different Kraft lignin/CA solutions in DMF/Ac. As can be observed, surface tension data remains at around 30.95–35.15 mN/cm for all Kraft lignins used, increasing the surface tension of DMF/Ac (23.64 mN/cm). This increment of surface tension could be attributed to improved interactions between the DMF/Ac and lignin/CA. It has been reported that in DMF, collapsed rigid spheres of lignin particles, rather than free and isolated lignin segments, would be generated due to intra- and intermolecular π-π interactions between the aromatic rings of lignin [77]. This happens since the attractive forces between lignin molecules are stronger than the dispersive forces of DMF molecules. The phenolic character of these Kraft lignins, previously observed by ^{13}C NMR and Folin-Ciocalteau reagent, tends to enhance these intra- and inter molecular interactions [78]. Several studies have established optimal surface tension values to facilitate electrospinnability of lignin solutions. Then, Ago et al. [32] established a surface tension value $\leq$43.2 mN/cm to obtain relatively uniform nanofibers by electrospinning from a solution of softwood Kraft lignin (50 wt%) in polyvinyl alcohol (PVA) (5 wt%). Du et al. [27] reported similar surface tension values (34.74 to 35.76 mN/cm) than that described herein when different organosolv lignins from poplar, pine and corn stalk (50 wt%) blended with polyacrylonitrile (PAN) were solubilized in DMF (20 wt% blend solution) and, subsequently electrospun to defect-free nanofibers.

Regarding the electrical conductivity of blend solutions, the addition of Kraft lignin/CA provides a fairly good electrical conductivity to DMF/Ac increasing from 3.2 μS/cm to 135.5–308.3 μS/cm, which are in a suitable range to obtain nanofibers [33]. The polar character of these lignins, due to their phenolic and aliphatic hydroxyl and carboxyl moieties among others, is mainly responsible for the electrical conductivity provided to DMF/Ac [34]. Moreover, the high residue percentages existing in the Kraft lignins (44 %–48 %), previously determined by TGA analysis, could also contribute to the electrical conductivity of DMF/Ac. Thus, the highest residue percentage contained in OTP lignin (48 %) resulted in the highest electrical conductivity for the OTP/CA solution (308.3 μS/cm), taking into account the major presence of Na_2SO_4, a strong electrolyte, as revealed FTIR analysis.

On the other hand, the viscosity of the solution has often been adjusted by varying the polymer concentration [79,80]. It has been established that a certain viscosity threshold corresponding to the critical polymer overlap concentration is desired to obtain relatively uniform nanofibers [81], and solutions with very high viscosity can be inappropriate for electrospinning [32]. Shear viscosity was determined from viscous flow tests for a concentration of 30 wt% and a lignin/CA ratio of 70:30. All the lignin/CA solutions studied exhibited a Newtonian behavior over the shear rate range applied (1–300 s^{-1}). Furthermore, compared to eucalypt and poplar (0.317 and 0.294 Pa·s), the addition of OTP led to the higher viscosity of the blend solution (0.475 Pa·s), which could be caused by its lower PDI [82] and higher C—C substructures [27] and higher amount of carbohydrates [83].

Table 6
Surface tension, electrical conductivity and shear viscosity of Kraft lignin/CA solutions.

Systems	Surface Tension (mN/m)	Electrical conductivity (μS/cm)	η (Pa·s)
Eucalypt/CA	31.15 ± 0.11	135.5 ± 0.10	0.317 ± 0.01
Poplar/CA	30.95 ± 0.16	141.3 ± 0.10	0.294 ± 0.02
OTP/CA	35.15 ± 0.07	308.3 ± 0.30	0.475 ± 0.02

3.7. Morphology and thermal properties of electrospun Kraft lignin/CA nanostructures

Fig. 6 displays SEM images of the morphology of resulting lignin/CA electrospun nanostructures obtained by electrospinning as a function of the type of Kraft lignin at 1.00 K (a, d, g) and 10.00 K (b, e, h). In general, Kraft lignin cannot be electrospun into nanofibers due to the lack of chain structures and/or molecular entanglements caused by its relatively low molecular weight [36]. The addition of CA as doping agent improves lignin electrospinnability and nanofiber development, probably due to the hydrogen bonding between the hydroxyl groups of Kraft lignins and the acetyl groups of CA [37]. In this sense, the phenolic hydroxyl groups from lignin play a key role in these hydrogen interactions [78], establishing stronger hydrogen bonds than aliphatic hydroxyl groups. Then, Kraft lignins from eucalypt and poplar, with higher phenolic content than that OTP, could thus have better interactions with CA molecules and, consequently lead to better spinnability. In this regard, Kubo and Kadla [78], reported major hydrogen interactions between phenolic hydroxyl groups of a softwood Kraft lignin and polyethylene oxide (PEO) as doping agent, improving the miscibility of this Kraft lignin. In the same way, Du et al. [27] described how the higher phenolic hydroxyl content of an organosolv lignin from poplar, compared to pine and corn stalk, led to a better interaction with PAN as doping agent, which resulted in improved miscibility and spinnability of poplar lignin.

On the other hand, when CA is added to lignin a mesophasic nanoscale liquid crystalline architecture is produced due to the lignin disrupting the crystalline and noncrystalline order of the cellulosic phase, resulting in a two-phase structure [37]. As can be seen, electrospun nanostructures based on eucalypt/CA (Figs. 6a and b) and poplar/CA (Figs. 6d and e) show uniform cross-linked nanofibers with a few beaded fibers. However, OTP/CA electrospun nanostructure presents micrographs formed by micro-sized particles that are interconnected to each other by nanometer-sized fibers (see Fig. 6g and h). The fiber diameter distribution (FDD) is also illustrated in Fig. 6. As can be observed, all Kraft lignin/CA samples present a homogeneous distribution of fibers in the micrograph. The mean diameters of nanofibers, particle and porosity obtained from FDD for eucalypt/CA, poplar/CA and OTP/CA are displayed in Table 7. As can be observed, the eucalypt/CA and poplar/CA nanostructures exhibit very similar morphological properties, with both systems showing similar mean nanofiber diameters (0.61 and 0.54 μm, respectively) and porosity. These results are in agreement with the physicochemical properties presented by the solutions since there were no significant differences between the two systems. However, OTP/CA displays a smaller mean nanofiber diameter (0.33 μm), forming a very weak bond between fibers and particles, possibly due to the high shear viscosity and electrical conductivity of the OTP/CA solution, which hindered the electrospinning process and the formation of a stable Taylor cone [83–85].

The lignin chemical structure also plays a critical role in the development of Kraft lignin/CA systems morphology. Lignins with a higher linearity (corresponding to a higher content of aryl-ether linkages such as β-O-4' and vinyl-ether substructures, among others) and, consequently less branching (correlated with a higher content of C—C substructures such as β-β′ resinol, β-5′ phenylcoumaran an stilbene substructures, among others) show a better spinnability, resulting in nanostructures with higher average diameters [27,28]. It could be due to a better alignment along the doping agent improving the formation of intermolecular bonds between lignin and the doping agent molecules. Thus, the higher content of β-O-4 and vinyl-ether substructures, observed for both eucalypt and poplar Kraft lignins, could enhance the alignment along CA, improving the interaction between lignin and CA molecules and, consequently the miscibility and spinnability of both eucalypt and poplar Kraft lignins as well as the largest average diameters observed for the resulting nanostructures. On the contrary, the higher content of C—C substructures observed for OTP lignin could explain its

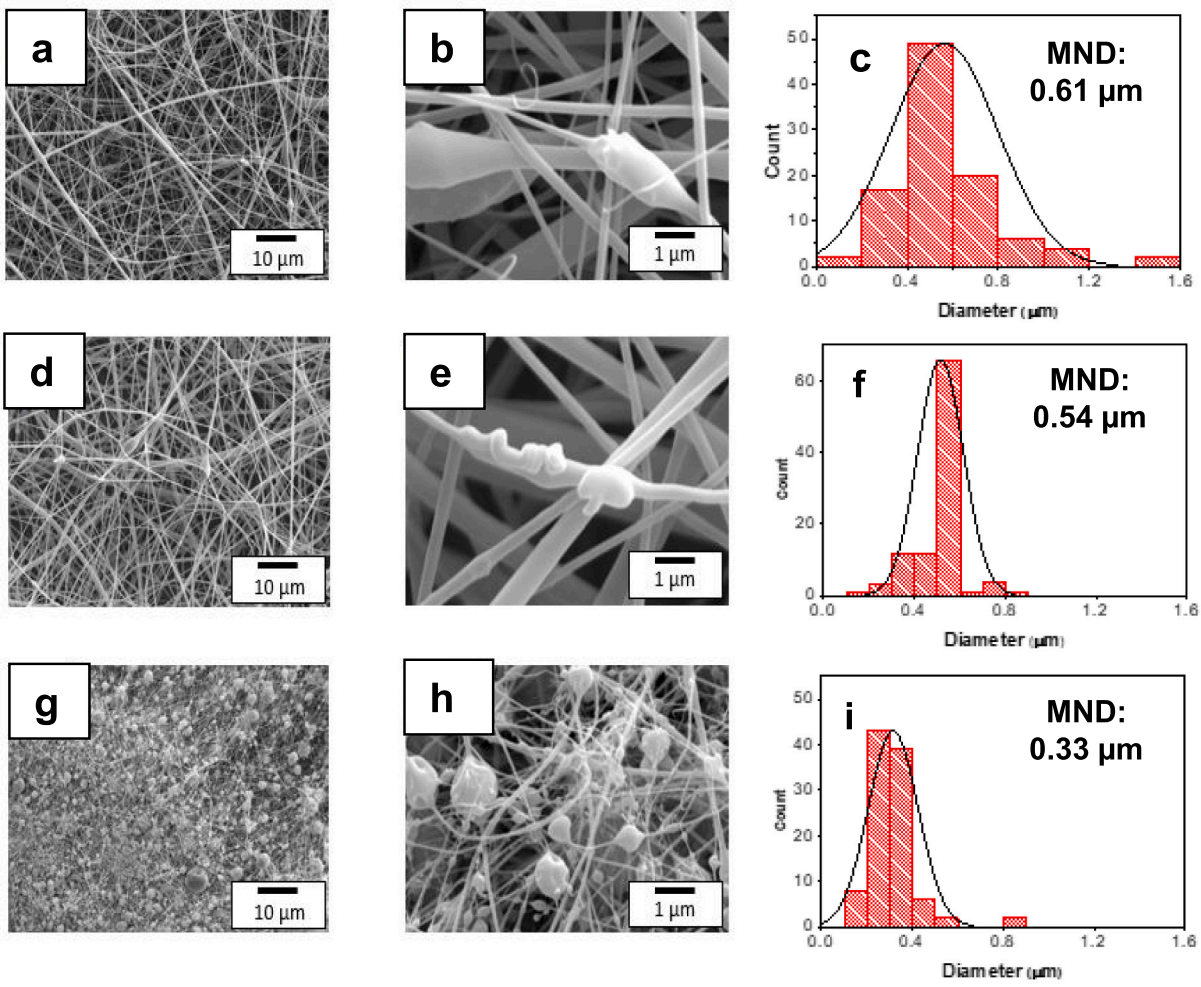

Fig. 6. SEM electrospun nanostructures obtained with different Kraft lignins and different magnifications: (a) eucalypt/CA at 1.00 k (b) eucalypt/CA at 10.00 k, (d) poplar/CA at 1.00 k, (e) poplar/CA at 10.00 k, (g) OTP/CA at 1.00 k and (h) OTP/CA at 10.00 k. Fiber size distribution from SEM electrospun nanostructures for eucalypt/CA (c), poplar/CA (f) and OTP/CA (i).

Table 7
Particle and fiber mean diameters and overall porosity of Kraft lignin/CA electrospun nanostructures.

Systems	Particle diameter (μm)	Fiber diameter (μm)	Porosity (%)
Eucalypt/CA	–	0.61	46.63
Poplar/CA	–	0.54	45.78
OTP/CA	0.97	0.33	37.19

worst performance during electrospinning process. In this sense, Du et al. [27] reported how the more linear structure with less branches observed for an organosolv poplar lignin, compared to organosolv lignins from pine and corn stalk, was beneficial to enhance its spinnability, obtaining nanofibers with the largest average diameters. Zhang et al. [28] also compared a soda lignin enriched in β-*O*-4 linkages with a Kraft lignin containing mostly highly stable C—C crosslinked structures (β-β′), observing a declined spinnability of the derived fibers from Kraft lignin. Moreover, the presence of polar lignin end-groups results in low spinnability of lignin [28]. Thus, the higher content of cinnamyl alcohol together with cinnamaldehyde observed for OTP lignin, compared to eucalypt and poplar Kraft lignins, could also support the worst performance of OTP during electrospinning process. Similar results were described by Zhang et al. [28], detecting many polar lignin end-groups in a Kraft lignin, such as guaiacyl propanol and coniferyl alcohol compared to a soda lignin, which in turn was unfavorable for spinnability of lignin.

Moreover, the abundance of S units is also beneficial to enhance the spinnability of lignin, while the H units is harmful, in which the content of methoxy groups is possibly essential reason [27]. Thus, the higher S/G ratios of eucalypt and poplar lignins compared to OTP Kraft lignin, which showed a content of H units (Table 3), could also explain the better electrospun nanostructures obtained from them. According to this, Du et al. [27] also described a higher S/G ratio for organosolv poplar lignin, compared to lignins containing mainly G and H units such as pine and corn stalk, resulting in the best electrospinning performance with independent filamentous morphology and uniform diameter.

Finally, the thermal properties of the electrospun Kraft lignin/CA nanostructures were evaluated (Fig. 5S). Fig. 5Sa and 5Sb correspond to TG and DTG, respectively, and denote that the electrospun nanostructure with the highest thermal stability is the poplar/CA system. On the other hand, as it is known, the addition of CA as a dopant increases the glass transition temperatures concerning Kraft lignins. Thus, in Fig. 5Sc (where DSC curves of electrospun Kraft lignin/CA nanostructures are shown) it can be seen that the highest Tg was obtained for the poplar/CA, followed by the eucalyptus/CA and finally the OTP/CA. All of these values are higher than those observed in Fig. 5c, where are showed the Tg of the different lignins without CA.

In general, the nanostructures produced from eucalypt and poplar Kraft lignin have suitable architectural parameters such as porosity,

geometry, diameter, interconnectivity, orientation and fiber distribution that make them potentially applicable as a thickening agent for the production of biodegradable oleogels [34,86].

4. Conclusions

Different micro- and nanostructures were obtained by electrospinning from Kraft lignins/cellulose acetate (CA) solutions in DMF/Ac. The addition of CA improves lignin electrospinnability and nanostructure development. The morphology of the electrospun nanostructures is affected by the intrinsic properties of the solution and the chemical structure of lignin. Eucalypt and poplar Kraft lignins showed a high purity (i.e., lower content of carbohydrates and salts) compared to OTP lignin (i.e., higher content of carbohydrates and salts). Moreover, eucalypt and poplar lignins displayed a higher content of β-O-4 substructures compared to OTP lignin, resulting in a major linearity, together with higher S/G ratios. All these factors led to a better spinnability of eucalypt and poplar lignins. Then, electrospun nanostructures based on eucalypt/CA and poplar/CA showed uniform cross-linked nanofibers with a few beaded fibers. However, OTP/CA electrospun nanostructure presented morphology with micro-sized particles that are interconnected to each other by nanometer-sized fibers. Therefore, understanding the physical-chemical properties and structural features of Kraft lignins would help to predict the ease of electrospinning each lignin and thus to find and optimize its possible applications such as vegetable oil thickening agents for the lubricant industry.

CRediT authorship contribution statement

Conceptualization; Concepción Valencia, María E., Eugenio, David Ibarra.

Data curation; Concepción Valencia, María E., Eugenio, David Ibarra.

Formal analysis; Luisa García-Fuentevilla, José F., Rubio-Valle, Raquel Martín-Sampedro, Concepción Valencia, María E., Eugenio, David Ibarra.

Funding acquisition; Concepción Valencia, María E., Eugenio, David Ibarra.

Investigation; Luisa García-Fuentevilla, José F., Rubio-Valle, Raquel Martín-Sampedro, Concepción Valencia, María E., Eugenio, David Ibarra.

Methodology; Luisa García-Fuentevilla, José F., Rubio-Valle, Raquel Martín-Sampedro, Concepción Valencia, María E., Eugenio, David Ibarra.

Project administration; Concepción Valencia, María E., Eugenio, David Ibarra.

Resources; Concepción Valencia, María E., Eugenio, David Ibarra.

Software; Luisa García-Fuentevilla, José F., Rubio-Valle, Raquel Martín-Sampedro, Concepción Valencia, María E., Eugenio, David Ibarra.

Supervision; Concepción Valencia, María E., Eugenio, David Ibarra.

Validation; Concepción Valencia, María E., Eugenio, David Ibarra.

Visualization; Luisa García-Fuentevilla, José F., Rubio-Valle, Raquel Martín-Sampedro, Concepción Valencia, María E., Eugenio, David Ibarra.

Roles/Writing - original draft; Concepción Valencia, María E., Eugenio, David Ibarra.

Writing – review &editing: Luisa García-Fuentevilla, José F., Rubio-Valle, Raquel Martín-Sampedro, Concepción Valencia, María E., Eugenio, David Ibarra.

Acknowledgments

This work is part of two coordinated research projects (RTI2018-096080-B-C21 and RTI2018-096080-B-C22) funded by MCIN/AEI/10.13039/501100011033 and by "ERDF A way of making Europe". The authors also wish to thank the Comunidad de Madrid and MCIU/AEI/FEDER, EU for funding this study via Projects SUSTEC-CM S2018/EMT-4348. The authors also acknowledge the pre-doctoral grants from José Fernando Rubio Valle (Ref. PRE2019-090632). The contribution of COST Action LignoCOST (CA17128), supported by COST (European Cooperation in Science and Technology), in promoting interaction, exchange of knowledge and collaborations in the field of lignin valorization is gratefully acknowledged.

Appendix A. Supplementary data

Supplementary data to this article can be found online at https://doi.org/10.1016/j.ijbiomac.2022.06.121.

References

[1] S. van Renssen, A bioeconomy to fight climate change, Nat. Clim. Chang. 4 (2014) 951–953, https://doi.org/10.1038/nclimate2419.
[2] R.S. Zalesny, D.M. Donner, D.R. Coyle, W.L. Headlee, An approach for siting poplar energy production systems to increase productivity and associated ecosystem services, For. Ecol. Manag. 284 (2012) 45–58, https://doi.org/10.1016/j.foreco.2012.07.022.
[3] H. Sixto, I. Cañellas, J. van Arendonk, P. Ciria, F. Camps, M. Sánchez, M. Sánchez-González, Growth potential of different species and genotypes for biomass production in short rotation in Mediterranean environments, For. Ecol. Manag. 354 (2015) 291–299, https://doi.org/10.1016/j.foreco.2015.05.038.
[4] J.M. Romero-García, L. Niño, C. Martínez-Patiño, C. Álvarez, E. Castro, M.J. Negro, Biorefinery based on olive biomass. State of the art and future trends, Bioresour. Technol. 159 (2014) 421–432, https://doi.org/10.1016/j.biortech.2014.03.062.
[5] J.M. Oliva, M.J. Negro, C. Álvarez, P. Manzanares, A.D. Moreno, Fermentation strategies for the efficient use of olive tree pruning biomass from a flexible biorefinery approach, Fuel 277 (2020), 118171, https://doi.org/10.1016/j.fuel.2020.118171.
[6] L. Jiménez-López, R. Martín-Sampedro, M.E. Eugenio, J.I. Santos, H. Sixto, I. Cañellas, D. Ibarra, Co-production of soluble sugars and lignin from short rotation white poplar and black locust crops, Wood Sci. Technol. 54 (2020) 1617–1643, https://doi.org/10.1007/s00226-020-01217-x.
[7] Ú. Fillat, B. Wicklein, R. Martín-Sampedro, D. Ibarra, E. Ruiz-Hitzky, C. Valencia, A. Sarrión, E. Castro, M.E. Eugenio, Assessing cellulose nanofiber production from olive tree pruning residue, Carbohydr. Polym. 179 (2018) 252–261, https://doi.org/10.1016/j.carbpol.2017.09.072.
[8] D. Ibarra, R. Martín-Sampedro, B. Wicklein, Ú. Fillat, M.E. Eugenio, Production of microfibrillated cellulose from fast-growing poplar and olive tree pruning by physical pretreatment, Appl. Sci. 11 (2021) 6445, https://doi.org/10.3390/app11146445.
[9] A.J. Ragauskas, G.T. Beckham, M.J. Biddy, R. Chandra, F. Chen, M.F. Davis, B. H. Davison, R.A. Dixon, P. Gilna, M. Keller, P. Langan, A.K. Naskar, J.N. Saddler, T. J. Tschaplinski, G.A. Tuskan, C.E. Wyman, Lignin valorization: improving lignin processing in the biorefinery, Science 344 (2014), https://doi.org/10.1126/science.1246843.
[10] A. Susmozas, R. Martín-Sampedro, D. Ibarra, M.E. Eugenio, R. Iglesias, P. Manzanares, A.D. Moreno, Process strategies for the transition of 1G to advanced bioethanol production, Processes 8 (2020) 1310, https://doi.org/10.3390/pr8101310.
[11] J. Ralph, K. Lundquist, G. Brunow, F. Lu, H. Kim, P.F. Schatz, J.M. Marita, R. D. Hatfield, S.A. Ralph, J.H. Christensen, W. Boerjan, Lignins: natural polymers from oxidative coupling of 4-hydroxyphenyl- propanoids, Phytochem. Rev. 3 (2004) 29–60, https://doi.org/10.1023/B:PHYT.0000047809.65444.a4.
[12] D.S. Bajwa, G. Pourhashem, A.H. Ullah, S.G. Bajwa, A concise review of current lignin production, applications, products and their environmental impact, Ind. Crop. Prod. 139 (2019), 111526, https://doi.org/10.1016/j.indcrop.2019.111526.
[13] J.J. Liao, N.H.A. Latif, D. Trache, N. Brosse, M.H. Hussin, Current advancement on the isolation, characterization and application of lignin, Int. J. Biol. Macromol. 162 (2020) 985–1024, https://doi.org/10.1016/j.ijbiomac.2020.06.168.
[14] P. Sannigrahi, Y. Pu, A. Ragauskas, Cellulosic biorefineries—unleashing lignin opportunities, Curr. Opin. Environ. Sustain. 2 (2010) 383–393, https://doi.org/10.1016/j.cosust.2010.09.004.
[15] P. Ortiz-Serna, M. Carsí, M. Culebras, M.N. Collins, M.J. Sanchis, Exploring the role of lignin structure in molecular dynamics of lignin/bio-derived thermoplastic elastomer polyurethane blends, Int. J. Biol. Macromol. 158 (2020) 1369–1379, https://doi.org/10.1016/j.ijbiomac.2020.04.261.
[16] M. Pishnamazi, H.Y. Ismail, S. Shirazian, J. Iqbal, G.M. Walker, M.N. Collins, Application of lignin in controlled release: development of predictive model based on artificial neural network for API release, Cellulose 26 (2019) 6165–6178, https://doi.org/10.1007/s10570-019-02522-w.
[17] M. Fodil Cherif, D. Trache, F. Benaliouche, S. Chelouche, A.F. Tarchoun, A. Mezroua, Effect of kraft lignins on the stability and thermal decomposition kinetics of nitrocellulose, Thermochim. Acta 692 (2020), 178732, https://doi.org/10.1016/j.tca.2020.178732.
[18] S. Beisl, A. Friedl, A. Miltner, Lignin from micro- to nanosize: applications, Int. J. Mol. Sci. 18 (2017) 2367, https://doi.org/10.3390/ijms18112367.

[19] M. Culebras, G.A. Collins, A. Beaucamp, H. Geaney, M.N. Collins, Lignin/Si hybrid carbon nanofibers towards highly efficient sustainable Li-ion anode materials, Eng. Sci. (2022), https://doi.org/10.30919/es8d608.
[20] J.F. Rubio-Valle, M. Jiménez-Rosado, V. Perez-Puyana, A. Guerrero, A. Romero, Electrospun nanofibres with antimicrobial activities, in: Antimicrob. Text. From Nat. Resour, Elsevier, 2021, pp. 589–618, https://doi.org/10.1016/B978-0-12-821485-5.00020-2.
[21] R. Ruiz-Rosas, J. Bedia, M. Lallave, I.G. Loscertales, A. Barrero, J. Rodríguez-Mirasol, T. Cordero, The production of submicron diameter carbon fibers by the electrospinning of lignin, Carbon N. Y. 48 (2010) 696–705, https://doi.org/10.1016/j.carbon.2009.10.014.
[22] N. Tucker, J.J. Stanger, M.P. Staiger, H. Razzaq, K. Hofman, The history of the science and technology of electrospinning from 1600 to 1995, J. Eng. Fiber. Fabr. 7 (2012), 155892501200702, https://doi.org/10.1177/155892501200702S10.
[23] N. Bhardwaj, S.C. Kundu, Electrospinning: a fascinating fiber fabrication technique, Biotechnol. Adv. 28 (2010) 325–347, https://doi.org/10.1016/j.biotechadv.2010.01.004.
[24] D. Li, Y. Xia, Electrospinning of nanofibers: reinventing the wheel? Adv. Mater. 16 (2004) 1151–1170, https://doi.org/10.1002/adma.200400719.
[25] S. Aslanzadeh, B. Ahvazi, Y. Boluk, C. Ayranci, Morphologies of electrospun fibers of lignin in poly(ethylene oxide)/N, N-dimethylformamide, J. Appl. Polym. Sci. 133 (2016), https://doi.org/10.1002/app.44172.
[26] J.D. Schiffman, C.L. Schauer, A. Review, Electrospinning of biopolymer nanofibers and their applications, Polym. Rev. 48 (2008) 317–352, https://doi.org/10.1080/15583720802022182.
[27] B. Du, H. Zhu, L. Chai, J. Cheng, X. Wang, X. Chen, J. Zhou, R.-C. Sun, Effect of lignin structure in different biomass resources on the performance of lignin-based carbon nanofibers as supercapacitor electrode, Ind. Crop. Prod. 170 (2021), 113745, https://doi.org/10.1016/j.indcrop.2021.113745.
[28] R. Zhang, Q. Du, L. Wang, Z. Zheng, L. Guo, X. Zhang, X. Yang, H. Yu, Unlocking the response of lignin structure for improved carbon fiber production and mechanical strength, Green Chem. 21 (2019) 4981–4987, https://doi.org/10.1039/C9GC01632E.
[29] I. Dallmeyer, F. Ko, J.F. Kadla, Electrospinning of technical lignins for the production of fibrous networks, J. Wood Chem. Technol. 30 (2010) 315–329, https://doi.org/10.1080/02773813.2010.527782.
[30] I. Dallmeyer, F. Ko, J.F. Kadla, Correlation of elongational fluid properties to fiber diameter in electrospinning of softwood kraft lignin solutions, Ind. Eng. Chem. Res. 53 (2014) 2697–2705, https://doi.org/10.1021/ie403724y.
[31] C. Lai, Z. Zhou, L. Zhang, X. Wang, Q. Zhou, Y. Zhao, Y. Wang, X.-F. Wu, Z. Zhu, H. Fong, Free-standing and mechanically flexible mats consisting of electrospun carbon nanofibers made from a natural product of alkali lignin as binder-free electrodes for high-performance supercapacitors, J. Power Sources 247 (2014) 134–141, https://doi.org/10.1016/j.jpowsour.2013.08.082.
[32] M. Ago, K. Okajima, J.E. Jakes, S. Park, O.J. Rojas, Lignin-based electrospun nanofibers reinforced with cellulose nanocrystals, Biomacromolecules 13 (2012) 918–926, https://doi.org/10.1021/bm201828g.
[33] M. Borrego, J.E. Martín-Alfonso, M.C. Sánchez, C. Valencia, J.M. Franco, Electrospun lignin-PVP nanofibers and their ability for structuring oil, Int. J. Biol. Macromol. 180 (2021) 212–221, https://doi.org/10.1016/j.ijbiomac.2021.03.069.
[34] J.F. Rubio-Valle, M.C. Sánchez, C. Valencia, J.E. Martín-Alfonso, J.M. Franco, Electrohydrodynamic processing of PVP-doped kraft lignin micro- and nano-structures and application of electrospun nanofiber templates to produce oleogels, Polymers (Basel) 13 (2021) 2206, https://doi.org/10.3390/polym13132206.
[35] A.A. Adam, J. Ojur Dennis, Y. Al-Hadeethi, E.M. Mkawi, B. Abubakar Abdulkadir, F. Usman, Y. Mudassir Hassan, I.A. Wadi, M. Sani, State of the art and new directions on electrospun lignin/cellulose nanofibers for supercapacitor application: a systematic literature review, Polymers (Basel) 12 (2020) 2884, https://doi.org/10.3390/polym12122884.
[36] H. Jia, N. Sun, M. Dirican, Y. Li, C. Chen, P. Zhu, C. Yan, J. Zang, J. Guo, J. Tao, J. Wang, F. Tang, X. Zhang, Electrospun kraft lignin/cellulose acetate-derived nanocarbon network as an anode for high-performance sodium-ion batteries, ACS Appl. Mater. Interfaces 10 (2018) 44368–44375, https://doi.org/10.1021/acsami.8b13033.
[37] M. Schreiber, S. Vivekanandhan, A.K. Mohanty, M. Misra, Iodine treatment of lignin-cellulose acetate electrospun fibers: enhancement of green fiber carbonization, ACS Sustain. Chem. Eng. 3 (2015) 33–41, https://doi.org/10.1021/sc500481k.
[38] D. Ibarra, R. Martín-Sampedro, B. Wicklein, A.M. Borrero-López, C. Valencia, A. Valdehíta, J.M. Navas, M.E. Eugenio, Populus alba L., an autochthonous species of Spain: a source for cellulose nanofibers by chemical pretreatment, Polymers (Basel) 14 (2021) 68, https://doi.org/10.3390/polym14010068.
[39] NRLE, TP-510-42618 - Determination of Structural Carbohydrates and Lignin in Biomass, Chem. Anal. Test. Lab. Anal. Proced. Natl. Renew. Energy Lab, 2011.
[40] A.M. Borrero-López, R. Martín-Sampedro, D. Ibarra, C. Valencia, M.E. Eugenio, J. M. Franco, Evaluation of lignin-enriched side-streams from different biomass conversion processes as thickeners in bio-lubricant formulations, Int. J. Biol. Macromol. 162 (2020) 1398–1413, https://doi.org/10.1016/j.ijbiomac.2020.07.292.
[41] R. Erdem, M. İlhan, E. Sancak, Analysis of EMSE and mechanical properties of sputter coated electrospun nanofibers, Appl. Surf. Sci. 380 (2016) 326–330, https://doi.org/10.1016/j.apsusc.2015.11.204.
[42] J. Rencoret, A. Gutiérrez, E. Castro, J.C. del Río, Structural characteristics of lignin in pruning residues of olive tree (Olea europaea L.), Holzforschung 73 (2018) 25–34, https://doi.org/10.1515/hf-2018-0077.
[43] J. Rencoret, G. Marques, A. Gutiérrez, D. Ibarra, J. Li, G. Gellerstedt, J.I. Santos, J. Jiménez-Barbero, Á.T. Martínez, J.C. del Río, Structural characterization of milled wood lignins from different eucalypt species, Holzforschung 62 (2008), https://doi.org/10.1515/HF.2008.096.
[44] T.-Q. Yuan, S.-N. Sun, F. Xu, R.-C. Sun, Structural characterization of lignin from triploid of Populus tomentosa Carr, J. Agric. Food Chem. 59 (2011) 6605–6615, https://doi.org/10.1021/jf2003865.
[45] E. Brännvall, 1. Overview of pulp and paper processes, in: Pulping Chem. Technol, De Gruyter, 2009, pp. 1–12, https://doi.org/10.1515/9783110213423.1.
[46] M. Alekhina, O. Ershova, A. Ebert, S. Heikkinen, H. Sixta, Softwood kraft lignin for value-added applications: fractionation and structural characterization, Ind. Crop. Prod. 66 (2015) 220–228, https://doi.org/10.1016/j.indcrop.2014.12.021.
[47] M. Lawoko, G. Henriksson, G. Gellerstedt, Characterisation of lignin-carbohydrate complexes (LCCs) of spruce wood (Picea abies L.) isolated with two methods, Holzforschung 60 (2006) 156–161, https://doi.org/10.1515/HF.2006.025.
[48] C. Fernández-Costas, S. Gouveia, M.A. Sanromán, D. Moldes, Structural characterization of kraft lignins from different spent cooking liquors by 1D and 2D nuclear magnetic resonance spectroscopy, Biomass Bioenergy 63 (2014) 156–166, https://doi.org/10.1016/j.biombioe.2014.02.020.
[49] R. Martín-Sampedro, J.I. Santos, Ú. Fillat, B. Wicklein, M.E. Eugenio, D. Ibarra, Characterization of lignins from Populus alba L. generated as by-products in different transformation processes: kraft pulping, organosolv and acid hydrolysis, Int. J. Biol. Macromol. 126 (2019), https://doi.org/10.1016/j.ijbiomac.2018.12.158.
[50] M.E. Eugenio, R. Martín-Sampedro, J.I. Santos, B. Wicklein, D. Ibarra, Chemical, thermal and antioxidant properties of lignins solubilized during Soda/AQ pulping of orange and olive tree pruning residues, Molecules 26 (2021) 3819, https://doi.org/10.3390/molecules26133819.
[51] M.E. Eugenio, R. Martín-Sampedro, J.I. Santos, B. Wicklein, J.A. Martín, D. Ibarra, Properties versus application requirements of solubilized lignins from an elm clone during different pre-treatments, Int. J. Biol. Macromol. 181 (2021) 99–111, https://doi.org/10.1016/j.ijbiomac.2021.03.093.
[52] N. Giummarella, P.A. Lindén, D. Areskogh, M. Lawoko, Fractional profiling of kraft lignin structure: unravelling insights on lignin reaction mechanisms, ACS Sustain. Chem. Eng. 8 (2020) 1112–1120, https://doi.org/10.1021/acssuschemeng.9b06027.
[53] N. Giummarella, I.V. Pylypchuk, O. Sevastyanova, M. Lawoko, New structures in eucalyptus kraft lignin with complex mechanistic implications, ACS Sustain. Chem. Eng. (2020), https://doi.org/10.1021/acssuschemeng.0c03776 acssuschemeng.0c03776.
[54] D. Ibarra, M.I. Chávez, J. Rencoret, J.C. Del Río, A. Gutiérrez, J. Romero, S. Camarero, M.J. Martínez, J. Jiménez-Barbero, A.T. Martínez, Lignin modification during eucalyptus globulus kraft pulping followed by totally chlorine-free bleaching: a two-dimensional nuclear magnetic resonance, fourier transform infrared, and pyrolysis−gas chromatography/mass spectrometry study, J. Agric. Food Chem. 55 (2007) 3477–3490, https://doi.org/10.1021/jf063728t.
[55] C.S. Lancefield, H.L.J. Wienk, R. Boelens, B.M. Weckhuysen, P.C.A. Bruijnincx, Identification of a diagnostic structural motif reveals a new reaction intermediate and condensation pathway in kraft lignin formation, Chem. Sci. 9 (2018) 6348–6360, https://doi.org/10.1039/C8SC02000K.
[56] P. Prinsen, J. Rencoret, A. Gutiérrez, T. Liitiä, T. Tamminen, J.L. Colodette, M.Á. Berbis, J. Jiménez-Barbero, Á.T. Martínez, J.C. del Río, Modification of the lignin structure during alkaline delignification of eucalyptus wood by kraft, soda-AQ, and soda-O 2 cooking, Ind. Eng. Chem. Res. 52 (2013) 15702–15712, https://doi.org/10.1021/ie401364d.
[57] L. Ralph, S.A., J. Ralph, Landucci, Database of Lignin and Cell Wall Model Compounds 2006, US For. Prod. Lab., Madison, WI, 2006. Available at Services/docs.htm?docids10491, access.
[58] J.I. Santos, Ú. Fillat, R. Martín-Sampedro, M.E. Eugenio, M.J. Negro, I. Ballesteros, A. Rodríguez, D. Ibarra, Evaluation of lignins from side-streams generated in an olive tree pruning-based biorefinery: bioethanol production and alkaline pulping, Int. J. Biol. Macromol. 105 (2017), https://doi.org/10.1016/j.ijbiomac.2017.07.030.
[59] C. Zhao, J. Huang, L. Yang, F. Yue, F. Lu, Revealing structural differences between alkaline and kraft lignins by HSQC NMR, Ind. Eng. Chem. Res. 58 (2019) 5707–5714, https://doi.org/10.1021/acs.iecr.9b00499.
[60] C. Zhao, Z. Hu, L. Shi, C. Wang, F. Yue, S. Li, H. Zhang, F. Lu, Profiling of the formation of lignin-derived monomers and dimers from eucalyptus alkali lignin, Green Chem. 22 (2020) 7366–7375, https://doi.org/10.1039/D0GC01658F.
[61] M.Y. Balakshin, E.A. Capanema, H.S.Gracz Chen, Elucidation of the structures of residual and dissolved pine kraft lignins using an HMQC NMR technique, J. Agric. Food Chem. 51 (2003) 6116–6127, https://doi.org/10.1021/jf034372d.
[62] H. Wang, Z. Liu, L. Hui, L. Ma, X. Zheng, J. Li, Y. Zhang, Understanding the structural changes of lignin in poplar following steam explosion pretreatment, Holzforschung 74 (2020) 275–285, https://doi.org/10.1515/hf-2019-0087.
[63] J.I. Santos, R. Martín-Sampedro, Ú. Fillat, J.M. Oliva, M.J. Negro, M. Ballesteros, M.E. Eugenio, D. Ibarra, Evaluating lignin-rich residues from biochemical ethanol production of wheat straw and olive tree pruning by FTIR and 2D-NMR, Int. J. Polym. Sci. 2015 (2015) 1–11, https://doi.org/10.1155/2015/314891.
[64] A. Martínez, G. Almendros, F. González-Vila, R. Fründ, Solid-state spectroscopic analysis of lignins from several Austral hardwoods, Solid State Nucl. Magn. Reson. 15 (1999) 41–48, https://doi.org/10.1016/S0926-2040(99)00045-4.
[65] M. Fodil Cherif, D. Trache, N. Brosse, F. Benaliouche, A.F. Tarchoun, Comparison of the physicochemical properties and thermal stability of organosolv and kraft lignins from hardwood and softwood biomass for their potential valorization,

Waste Biomass Valoriz. 11 (2020) 6541–6553, https://doi.org/10.1007/s12649-020-00955-0.
[66] M. El Moustaqim, A. El Kaihal, M. El Marouani, S. Men-La-Yakhaf, M. Taibi, S. Sebbahi, S. El Hajjaji, F. Kifani-Sahban, Thermal and thermomechanical analyses of lignin, Sustain. Chem. Pharm. 9 (2018) 63–68, https://doi.org/10.1016/j.scp.2018.06.002.
[67] S.H.F. da Silva, P.S.B. dos Santos, D. Thomas da Silva, R. Briones, D.A. Gatto, J. Labidi, Kraft lignin-based polyols by microwave: optimizing reaction conditions, J. Wood Chem. Technol. 37 (2017) 343–358, https://doi.org/10.1080/02773813.2017.1303513.
[68] C. Liu, H. Wang, A.M. Karim, J. Sun, Y. Wang, Catalytic fast pyrolysis of lignocellulosic biomass, Chem. Soc. Rev. 43 (2014) 7594–7623, https://doi.org/10.1039/C3CS60414D.
[69] J. Hu, R. Xiao, D. Shen, H. Zhang, Structural analysis of lignin residue from black liquor and its thermal performance in thermogravimetric-fourier transform infrared spectroscopy, Bioresour. Technol. 128 (2013) 633–639, https://doi.org/10.1016/j.biortech.2012.10.148.
[70] D.R. de Oliveira, I.de M. Nogueira, F.J.N. Maia, M.F. Rosa, S.E. Mazzetto, D. Lomonaco, Ecofriendly modification of acetosolv lignin from oil palm biomass for improvement of PMMA thermo-oxidative properties, J. Appl. Polym. Sci. 134 (2017) 45498, https://doi.org/10.1002/app.45498.
[71] H. Yang, R. Yan, H. Chen, D.H. Lee, C. Zheng, Characteristics of hemicellulose, cellulose and lignin pyrolysis, Fuel 86 (2007) 1781–1788, https://doi.org/10.1016/j.fuel.2006.12.013.
[72] O. Gordobil, R. Moriana, L. Zhang, J. Labidi, O. Sevastyanova, Assesment of technical lignins for uses in biofuels and biomaterials: structure-related properties, proximate analysis and chemical modification, Ind. Crop. Prod. 83 (2016) 155–165, https://doi.org/10.1016/j.indcrop.2015.12.048.
[73] A. García-Maraver, L.C. Terron, A. Ramos-Ridao, M. Zamorano, Effects of mineral contamination on the ash content of olive tree residual biomass, Biosyst. Eng. 118 (2014) 167–173, https://doi.org/10.1016/j.biosystemseng.2013.12.009.
[74] C. Huang, J. He, R. Narron, Y. Wang, Q. Yong, Characterization of kraft lignin fractions obtained by sequential ultrafiltration and their potential application as a biobased component in blends with polyethylene, ACS Sustain. Chem. Eng. 5 (2017) 11770–11779, https://doi.org/10.1021/acssuschemeng.7b03415.
[75] M.N. Mohamad Ibrahim, N. Zakaria, C.S. Sipaut, O. Sulaiman, R. Hashim, Chemical and thermal properties of lignins from oil palm biomass as a substitute for phenol in a phenol formaldehyde resin production, Carbohydr. Polym. 86 (2011) 112–119, https://doi.org/10.1016/j.carbpol.2011.04.018.
[76] L. Hu, T. Stevanovic, D. Rodrigue, Unmodified and esterified kraft lignin-filled polyethylene composites: compatibilization by free-radical grafting, J. Appl. Polym. Sci. 132 (2015) n/a-n/a, https://doi.org/10.1002/app.41484.
[77] N. Alwadani, N. Ghavidel, P. Fatehi, Surface and interface characteristics of hydrophobic lignin derivatives in solvents and films, Colloids Surf. A Physicochem. Eng. Asp. 609 (2021), 125656, https://doi.org/10.1016/j.colsurfa.2020.125656.
[78] S. Kubo, J.F. Kadla, Hydrogen bonding in lignin: a fourier transform infrared model compound study, Biomacromolecules 6 (2005) 2815–2821, https://doi.org/10.1021/bm050288q.
[79] R.M. Nezarati, M.B. Eifert, E. Cosgriff-Hernandez, Effects of humidity and solution viscosity on electrospun fiber morphology, Tissue Eng. Part C Methods 19 (2013) 810–819, https://doi.org/10.1089/ten.tec.2012.0671.
[80] P. Gupta, C. Elkins, T.E. Long, G.L. Wilkes, Electrospinning of linear homopolymers of poly(methyl methacrylate): exploring relationships between fiber formation, viscosity, molecular weight and concentration in a good solvent, Polymer (Guildf). 46 (2005) 4799–4810, https://doi.org/10.1016/j.polymer.2005.04.021.
[81] S. Aslanzadeh, B. Ahvazi, Y. Boluk, C. Ayranci, Carbon fiber production from electrospun sulfur free softwood lignin precursors, J. Eng. Fiber. Fabr. 12 (2017), 155892501701200, https://doi.org/10.1177/155892501701200405.
[82] F. Ko, Y. Gogotsi, A. Ali, N. Naguib, H. Ye, G.L. Yang, C. Li, P. Willis, Electrospinning of continuous carbon nanotube-filled nanofiber yarns, Adv. Mater. 15 (2003) 1161–1165, https://doi.org/10.1002/adma.200304955.
[83] S. Seo, PN, S.Y. Han, C.W. Park, S.Y. Lee, N.H. Kim, Lee, Preparation and characterization of electrospun composite nanofibers from poly (vinyl alcohol)/lignocellulose nanofibrils with different chemical compositions, Bioresour. 14 (2019) 5764.
[84] W.J. Scheideler, C.-H. Chen, The minimum flow rate scaling of Taylor cone-jets issued from a nozzle, Appl. Phys. Lett. 104 (2014) 24103, https://doi.org/10.1063/1.4862263.
[85] F.J. Higuera, Flow rate and electric current emitted by a Taylor cone, J. Fluid Mech. 484 (2003), S0022112003004385, https://doi.org/10.1017/S0022112003004385.
[86] J. Wang, L. Tian, B. Luo, S. Ramakrishna, D. Kai, X.J. Loh, I.H. Yang, G.R. Deen, X. Mo, Engineering PCL/lignin nanofibers as an antioxidant scaffold for the growth of neuron and Schwann cell, Colloids Surf. B Biointerfaces 169 (2018) 356–365, https://doi.org/10.1016/j.colsurfb.2018.05.021.